5-21-2005

CDSE Quantum Dots and Luminescent/Magnetic Particles for Biological Applications

Desheng Wang
University of New Orleans

CDSE QUANTUM DOTS AND LUMINESCENT/MAGNETIC PARTICLES FOR BIOLOGICAL APPLICATIONS

A Thesis

Submitted to the Graduate Faculty of the
University of New Orleans
in partial fulfillment of the
requirements for the degree of

Master of Science
in
The Department of Chemistry

by

Desheng Wang

B.S, Nankai University, China, 1997

May 2004

ACKNOWLEDGEMENTS

This dissertation is dedicated to my advisor, Professor Zeev Rosenzweig. His wisdom, invaluable advices, support and encouragement have always been there for me whenever I need.

I sincerely thank Dr. Jibao He from Electron and Confocal Microscopy lab of Tulane University for his help on the TEM images.

I would like to thank Professor Nista Rosenzweig from Xavier University for her supply of cells and valuable advices on the experiments.

I would like to thank Professor Matthew Tarr, Professor Scott Whittenburg, Professor Ron Evilia and Professor John Wiley for their help on my study in University of New Orleans.

I would like to thank everyone in my group for their help and advices in the past two and half years. Especially Gabriela Blagoi, her unselfish dedication to the lab is one of the reasons that I could perform my work.

I also want to thank Susan for her caring and support.

This work is supported financially by the National Science Foundation (NSF) grant CHE-0314027 and the Department of Defense grant MDA972-03-C-0100.

TABLE OF CONTENTS

ABSTRACT iii

CHAPTER 1: BACKGROUND OF QUANTUM DOTS 1

1.1 What Are Quantum Dots 1

1.2 Fluorescence and Fluorescence Sensing 2

1.2.1. Jablonski Diagram 2

1.2.2. Fluorescence Quantum Yield and Lifetime 5

1.2.3. Semiconductor Fluorescence 5

1.3 Application of Quantum Dots 9

1.4 Cell Separation Using Magnetic Nanoparticles 11

CHAPTER 2: EXPERIMENTAL 13

2.1 Materials and Reagents 13

2.2 Synthesis of CdSe and CdSe/ZnS Quantum Dots 14

2.3. Surface Modification of Quantum Dots with Thiol Ligands 16

2.4. Oxygen Sensitivity of Water-Soluble Quantum Dots 17

2.5. Synthesis of Luminescent/Magnetic Particles 17

2.6. Protocol of EDAC Coupling 18

2.7. Characterizations 19

a) Absorption Spectra 19
b) Fluorescence Emission Spectra 20
c) Measurement of Quantum Yield.....20
d) Microscopy 20
e) Transmission Electron Microscopy 21
2.8. Biological Experiments.....21
2.8.1. Breast Cancer Cells (MCF-7) Preparation 21
2.8.2. Cells Labeling.....22
CHAPTER 3: RESULTS AND DISSCUSSIONS 24
3.1. Synthesis of CdSe and CdSe/ZnS Quantum Dots 24
3.2. Water Solubility of CdSe/ZnS Quantum Dots.....27
3.3. Oxygen Sensitivity of Water-Soluble CdSe/ZnS Quantum Dots 29
3.4. CdSe/ZnS Quantum Dots – Magnetic Beads Luminescent/Magnetic Particles.....31
3.5. Biological Application.....39
3.5.1. Breast Cancer Cells Labeling 39
3.5.2. Cells Separation 42
3.6. Summary 45
CHAPTER 4: SUMMARY AND CONCLUSIONS.....46
REFERENCES 48
VITA 53

ABSTRACT

CdSe semiconductor nanocrystals (quantum dots--QDs) with diameters ranging between 1.5 and 8 nm exhibit strong, tunable luminescence [1-5]. They have been widely investigated for their size-dependent optoelectronic properties [6], and for their potential use in optical devices [7], biological labels [8] and sensors [9]. Luminescent quantum dots (QDs) show higher photostability and narrower emission peaks compared to organic fluorophores [8]. The objective of my project was to apply QDs magnetic/luminescent nanoparticle as biological labels in cells. Luminescent CdSe QDs emit bright visible light with high quantum yield and sharp emission peak. The CdSe QDs were capped with a ZnS layer. This increased their emission efficiency and photostability due to the larger band gap of ZnS. The QDs were transferred from organic solvent (e.g. chloroform, hexane) to water by exchanging the capping group (Trioctylphosphine Oxide—TOPO) with mercaptoacetic acid. To develop a separation and detection tool for cells, we combined γ-Fe_2O_3 magnetic particles with CdSe/ZnS QDs in core-shell composite. The composite nanoparticles showed strong fluorescence emission and high water solubility. Different antibodies were attached to the particles through EDAC coupling. The antibody-coated particles were used to successfully separate and detect breast cancer cells in blood cells.

CHAPTER 1: BACKGROUND OF QUANTUM DOTS

1.1 What Are Quantum Dots?

Quantum dots are nanometer (10^{-9} meter) scale particles that are neither small molecules nor bulk solids. Their composition and small size (a few hundred to a few thousand atoms) give these dots extraordinary optical properties that can be readily customized by changing the size or composition of the dots. Quantum dots absorb light, and then emit the light but in a different color. Although other organic and inorganic materials exhibit this phenomenon — fluorescence — the ideal fluorophore would be bright, non-photobleaching with narrow, symmetric emission spectra, and have multiple resolvable colors that can be excited simultaneously using a single excitation wavelength. Quantum dots closely fit this ideal. [9]

Quantum dots (or QD nanocrystals) combine the most sought-after characteristics, such as multiple colors and brightness, offered by either fluorescent dyes or semiconductor LEDs (light emitting diodes). In addition, quantum dot particles have many unique optical properties that are found only in these materials. The most striking property is that the color of quantum dots — both in absorption and emission — can be "tuned" to any chosen wavelength by simply changing their size. The principle behind

this unique property is the quantum confinement effect. This leads to different-sized quantum dots emitting light of different wavelengths. By using only a small number of semiconductor materials and an array of different sizes, it is possible to prepare quantum dots with colors that span the spectrum, from ultraviolet to infrared.

1.2 Fluorescence and Fluorescence Sensing

Fluorescence is a luminescence phenomenon that usually occurs in poly-aromatic hydrocarbons or heterocycles molecules called fluorescent molecules. It is the process in which absorption of light of a given wavelength by a fluorescent molecule is followed by the emission of light at longer wavelengths. Fluorescence, chemiluminescence and phosphorescence are examples of luminescence, which are defined based on the nature of the excited state. Fluorescence occurs when the molecule returns to the electronic ground state from the excited singlet state with an emission of a photon. Phosphorescence is the emission of light from the spin forbidden transition of the electron from the triple state to the ground state. Chemiluminescence occurs when a chemical reaction produces an electronically excited species, which emits a photon in order to reach the ground state.

Below are several principles, which are important to understand the phenomenon of fluorescence and fluorescence sensing techniques.

1.2.1 Jablonski Diagram

Once a molecule absorbed electromagnetic radiation, there are a number of routes by which it can return to the ground state (statistically the most common energy state for room temperature chemical species). Jablonski diagram (Figure 1.1) illustrates the processes involved in the creation of an excited electronic state by optical absorption and subsequent emission.

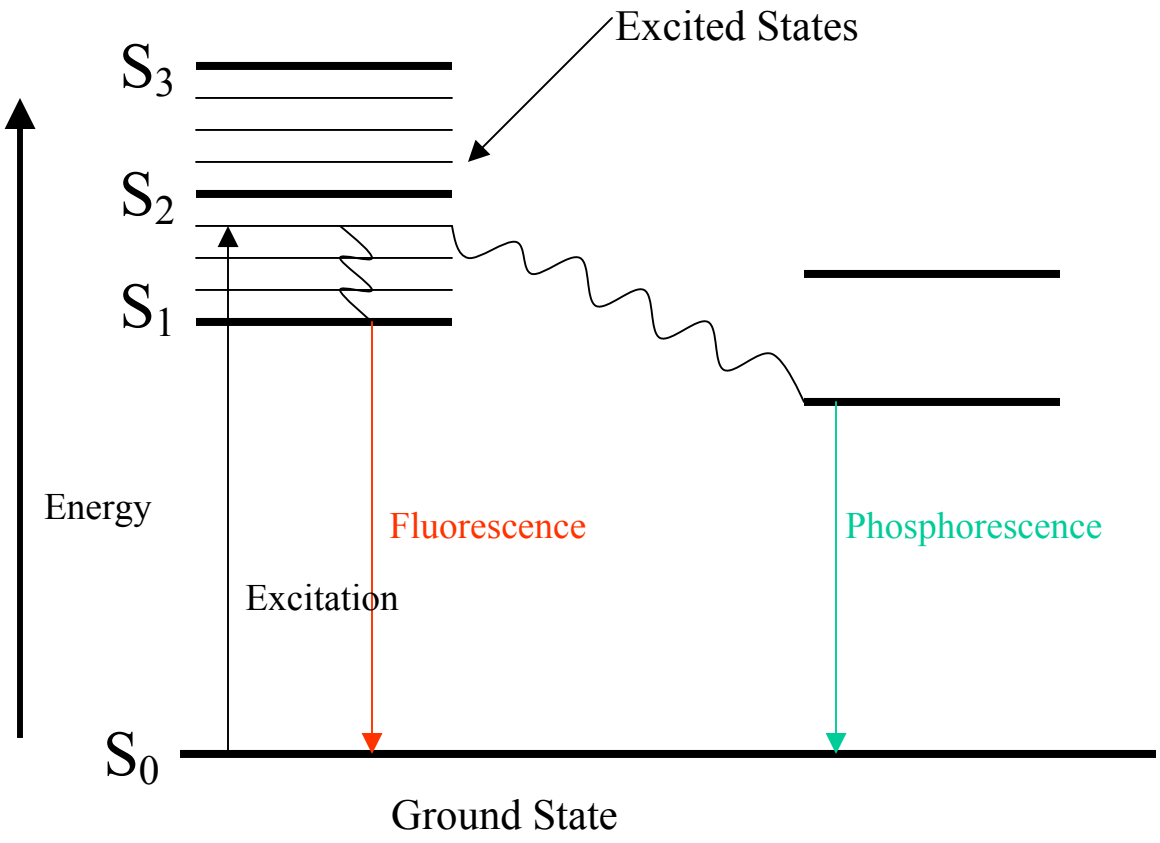

Figure 1.1 Jablonski diagram describing radiative and non-radiative transitions following excitation.

S_0, S_1, S_2, and S_n represent the singlet states of 1st, 2nd, and nth electronic energy levels. A number of vibrational energy levels exist in each of these electronic states. There are few processes occurring following the absorption of light. A fluorophore is

excited to higher vibrational levels of S_1 or S_2. The molecule is then relaxed to the lowest vibrational level of S_1 through a process called internal conversion, which occurs very quickly ($<1\times10^{-12}$ seconds). Returning to the ground state occurs, which then quickly reaches thermal equilibrium. Due to energy dissipation during the excited-state lifetime, the energy of emission photon $h\nu_{EM}$ is lower, and therefore of longer wavelength, than the excitation photon h_{EX}. The difference in energy or wavelength represented by ($h\nu_{EX} - h\nu_{EM}$) is called the Stokes shift. (figure 1.2) The Stokes shift is fundamental to the sensitivity of fluorescence techniques because it allows emission photons to be detected against a low background, isolated from excitation photons. If the photon emission occurs between states of the same spin state (e.g. S_1 ---> S_0), it is termed fluorescence. If the spin state of the initial and final energy levels is different (e.g. T_1 --> S_0), the emission is called phosphorescence. The fluorescence lifetimes are very short; about 1 x 10^{-5} to 10^{-8} seconds. The phosphorescence lifetimes are longer; about 1 x 10^{-4} seconds to minutes or even hours.

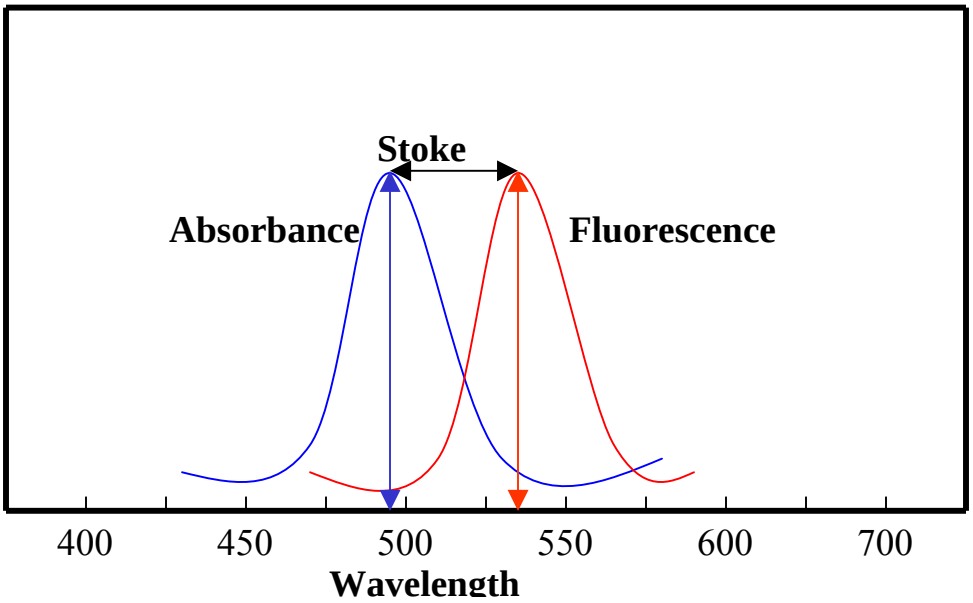

Figure 1.2. Fluorescence spectra

There are three significant nonradiative deactivation processes: internal conversion (IC), intersystem crossing (ISC) and vibrational relaxation. Internal conversion is the radiationless transition between energy states of the same spin state (compare with fluorescence-a radiative process). Intersystem crossing is a radiationless transition between different spin states (compare to phosphorescence). Vibrational relaxation, the most common of the three-for most molecules, occurs very quickly (<1 x 10^{-12} seconds). Vibrational relaxation is enhanced by physical contact of an excited molecule with other particles with which energy, in the form of vibrations and rotations, can be transferred through collisions.

1.2.2 Fluorescence quantum yield and lifetime

Fluorescence quantum yield (Q) is the ratio of the number of emitted photons to the number of absorbed photons. Substances with the large quantum yield display bright emission. Fluorescence lifetime (T_F) is the average length of time a molecule remains in its excited state. A fluorescence lifetime generally is near 10ns. The fluorescence lifetime determines the time available for the fluorophore to interact with or diffuse in its environment.

1.2.3 Semiconductor Fluorescence

There are two kinds of semiconductors based on their conductive mechanism, N (negative) type and P (positive) type. The optical properties of a semiconductor are critically controlled by its band gap between conduction band and valence band. In molecular terms, it is analogous to the lowest energy electronic transition where an

electron in the highest occupied molecular orbital (HOMO) is transferred to the lowest unoccupied molecular orbital (LUMO), as compared in figure 1.3. HOMO gives rise to electron filled valence band while LUMO gives rise to empty conduction band.

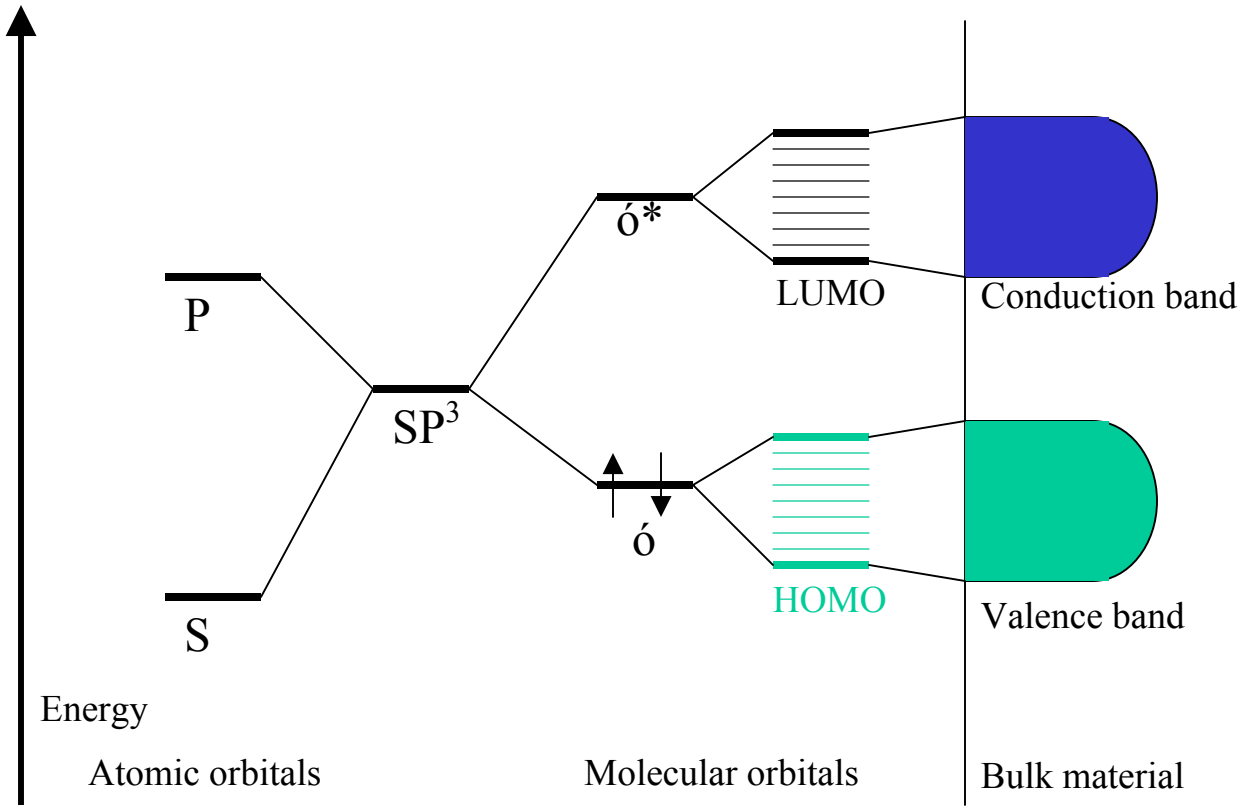

Figure 1.3 Silicon as a prototype semiconductor.

Semiconductor	Band-gap energy (ev)	Approximate threshold wavelength (nm)
Si	1.12	1107
Ge	0.66	1879
CdS	2.42	512
CdSe	1.70	729
CdTe	1.50	827
ZnS	3.2	388
ZnSe	2.58	481
PbS	0.50	2480
HgS	0.50	2480
HgTe	0.14	8857
GaAs	1.43	867

Table 1.1 Band gaps and optical properties of some semiconductors (Adapted from ref 11). All data are bulk material values and under room temperature.

Semiconductor fluorescence is analogous to molecular. In a semiconductor, radiation resulting in light emission or luminescence happens in electron-hole pair recombination processes (either band to band or mediated by states in the gap region or at the semiconductor surface). [11] After an electron absorbs enough energy to jump to the conduction band leaving a hole behind, it tends to return to the valence band with a fluorescence emission whose energy is lower than its excitation energy. Table 1.1 lists the values of band gap energy (Eg) and the wavelength cutoff limits of emission. Corresponding to the band gaps, there is a wide range of absorption from 388 nm to 8857 nm. Only a few of them like CdS and CdSe are in the visible light range (400-700 nm) of the electromagnetic spectrum.

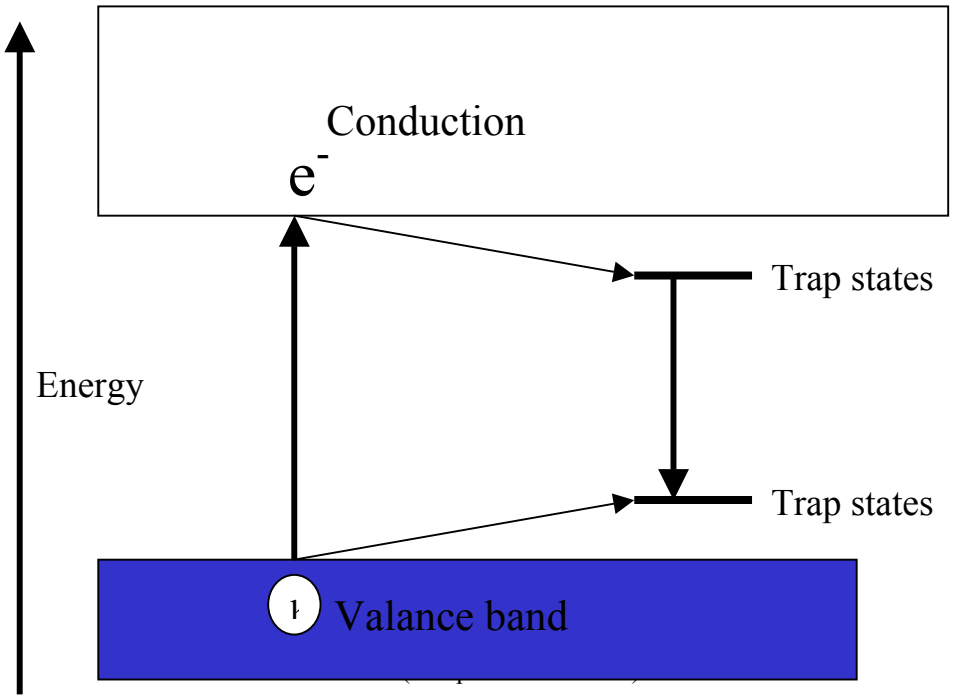

Figure 1.4 Energy description of semiconductor excitation

The electron must have a minimum *E*g band-gap energy to undergo this promotion. The created electron–hole pair, an exciton, may recombine immediately to produce heat or light with an energy equal to *E*g, but it is more likely that trap states within the material trap either the electron or the hole. (Figure 1.4) These trap states result from numerous factors, including structural defects, atomic vacancies, dangling bonds, and adsorbents at the interface. Radiative recombination of the trapped charge carriers then produces luminescence that is substantially red-shifted from the absorbed light. These trap states are very much related to the size and surface structure of the semiconductor. A very unique property of semiconductor quantum dots is the size dependence of luminescence emission. As mentioned, surface to volume ratio has a great affect on trap states of which the mechanism is not quite clear. The tendency is as size getting smaller the band gap becomes larger. So the fluorescence color can be tuned by changing the size of the quantum dots [12]. As the size of quantum dots gets smaller than their Bohr Radius, their unique chemical and electronic properties give rise to their potential use in the fields of nonlinear optics, luminescence, electronics, catalysis, solar energy conversion, and optoeletronics, as well as biological sensing.

1.3 Application of Quantum Dots

The potential applications of semiconductor quantum dots due to their size, tunable fluorescence, high quantum yield and wide excitation wavelength range have generated increasing interest among researchers in the past ten years. In 1994, Bawendi et al [27] reported the use of CdSe/TOPO nanocrystals in a thin film device. Other studies in various fields were soon to follow:

Optoelectronic Applications: The surface area of a nanocrystal and the surrounding medium such the capping reagent can have a profound effect on the properties of the particle [12]. Defects within the particle act as electron/hole traps which can lead to nonlinear optic effects [28]. New nonlinear composite materials can be prepared by doping either polymers or glasses with semiconductor nanocrystallites [29]. For example, Herron et al. [30] prepared polymer matrix composites containing PbS and CdSe nanocrystallites and showed the optical nonlinearity of material containing 5 nm sized CdS nonocrystals to be -6.1×10^{-7} cm^2W^{-1} at 480 nm.

Catalysis: the large surface area-to-volume ratio, along with the ability to tune the band gap by changing particle size, means that nonodispersed semiconductor can be used as catalysts in photochemical reactions. The redox levels of the conduction and valence bands are especially sensitive to size quantization effects; with charge carriers formed after light absorption migrating to the surface of the particles where they can reduce or oxidize surface-bound chemical species [31]. For example, Henglein et al. reported the use of ZnS nanoparticles for oxidation of alcohols and the reduction of CO_2 to formic acid [32].

Sensing: There has been great interest in this area including biological and chemical sensing [13,33-35]. For example, Kumar and Sberveglieri reported that TiO_2 nanoparticles can be used as sensors for the detection of O_2, NO_2, and organic molecules [36,37]. The selectivity of the sensor depends on the method used to produce the TiO_2 nanoparticles, with the efficiency of the chemical sensors increasing with decreasing particles size decreases. Nazzal et al. [13] found the photoluminescence of polymer thin films incorporated with high-quality CdSe nanocrystals respond rapidly to amine gases under photoirradiation. Another active area is biological sensing. Chan et al [35] used CdSe/ZnS QDs modified with a protein transferrin to label HeLa cells through receptor-mediated endocytosis. They demonstrated that the attached transferring molecules were still active and recognized by the receptors on the cell surface. Their report also showed that when QDs labeled with IgG incubated with bovine serum albumin (BSA) and a specific polyclonal antibody, the polyclonal antibody recognized the Fab fragments of the IgG and induced an extensive aggregation of CdSe/ZnS QDs. In another report, Jaiswal et al. [33] demonstrated that QDs could be used for multiple-color imaging of live cells. The labeling did not affect the normal growth and development of live cells, and have no obvious effect on cellular. Luminescent quantum dots also can be applied in quantitative bioanalysis. In protein and DNA chips, organic dyes have been widely used for drug screening and disease diagnostics. However, poor photostability and overlaps between emission peaks have been a problem. To overcome this problem, quantum dots have been explored as alternative of organic fluorophores in immunoassays and DNA analysis. Goldman et al. [38,39] prepared QDs-antibody conjugates and used them in fluoroimmunoassays for the detection of protein toxin and TNT with detection limits of

10 ng/ml for the toxin and 2 ng/ml for TNT. Han et al. [40] encapsulated CdSe/ZnS QDs into 1.2 μm porous polystyrene microbeads with different ratios of quantum dots of different emission colors and formed barcodes for DNA hybridization assays. They prepared quantum dots of six different emission colors and doped them into polymer beads with 10 different ratios of emission intensity. The QDs doped polymer beads could be used to analyze one million DNA samples in a single detection assay.

1.4 Cell Separation Using Magnetic Nanoparticles

Cell isolation is a fundamental and important cell preparation technique in a variety of biological and biomedical applications including the diagnosis and treatment of disease [54-58]. Magnetic cell separation has become a popular tool for the isolation of cells, especially rare cells, from a heterogeneous mixture. The magnitude of the magnetophoretic mobility of a magnetically tagged cell is a parameter that distinguishes this cell from unlabeled or untagged cells. Magnetic cell separation typically employs the use of antibodies against specific cell surface acceptors to tag cells of interest with magnetic particle conjugates.

Increasing interest in the potential biological application of magnetic particles resulted synthesis and characterization studies of these particles. Nu´n˜ez et al. [60] successfully synthesized Fe-based elongated alloy particles of about 120 × 20 nm protected with an alumina coating from a mixture precursor FeSO4 and $Co(NO_3)_2$ in the presence of NaOH and Na_2CO_3. The addition of cobalt retarded the formation of the goethite precursors. The presence of the alumina coating was essential to prevent

interparticle sintering and therefore to achieve higher values of coercivity. A novel magnetic support for Fe_3O_4 particles was prepared by an oxidization-precipitation method with poly (vinyl alcohol) (PVA) as the entrapment material [57]. The particles showed superparamagnetic properties and no aggregation. Tartaj et al. [61] successfully dispersed nanomagnets into colloidal silica cages. They proved that the particles could be used for chemical separation in medicine, biology, and environmental protection. Ferrofluids, which are colloidal solutions of ferro- or ferromagnetic nanoparticles in a carrier fluid, have been widely used [56,59]. Fauconnier et al. [56] coated dimercaptosuccinic acid on the surface of ferrofluid particles through S-S bridges forming a polymer layer. The particles had both free thiol (-SH) and carboxy (-COOH) groups on the surface. These particles showed high binding potential to antibodies [47].

CHAPTER 2: EXPERIMENTAL

This chapter describes the experimental methods and instruments used to carry out the studies that are summarized in this dissertation. Specific technical and experimental details are described in related chapters.

2.1 Materials and Reagents

Cadmium Oxide (CdO, Sigma)

Lauric Acid (Sigma)

Trioctylphosphine (TOP, Sigma)

Trioctylphophine Oxide (TOPO, Sigma)

hexadecylamine (HDA, Sigma)

Selenium powder (Sigma)

Diethylzinc ($Zn(Et)_2$, Sigma)

Hexamethyldisllathiane ($(TMS)_2S$, Sigma)

Mercaptoacetic acid (Sigma)

Dimercapto-succinimid acid (DMSA) coated γ-Fe_2O_3 magnetic particles (Indicia, France)

1-ethyl-3- (3-dimethylaminopropyl) carbodiimide (EDAC)

Mouse anti-cyclin E antibody (Zymed)

MCF7 breast cancer cells (ATCC)

Red blood cells (Sigma)

2.2 Synthesis of CdSe and CdSe/ZnS Quantum Dots

Luminescent CdSe/ZnS QDs of green emission and red emission colors were synthesized based on a method developed by Peng et al., with minor modifications [4]. 12.7 mg cadmium oxide and 160 mg lauric acid were mixed in a 100 ml three-neck flask. The mixture was heated to >200 °C in a mantle to fully dissolve the cadmium oxide in the lauric acid solution forming a clear colorless solution. A higher temperature (<320 °C) will speed up the dissolving. At 280 °C, it usually takes 10-15 minutes to fully dissolve the cadmium oxide. Then, 1.94 g trioctylphosphine oxide (TOPO) and 1.94 g hexadecylamine (HDA) were added to the solution under stirring. The mixture was heated to a temperature higher than 280 °C which depends on the desired size or color of QDs, and kept under a dry nitrogen atmosphere. Upon reaching the desirable temperature the mantle was removed and 2 ml trioctylphosphine (TOP) solution containing 80 mg selenium powder was rapidly injected into the solution under vigorous stirring. It was previously shown that the diameter of the formed QDs depends on the reaction temperature with smaller particles formed at higher temperature [1]. The color of the mixture changed from clear colorless to green, orange or red depending on the exact temperature. As the QDs growing, the color also changed from green to red, and even deep red.

To form ZnS, two different procedures can be used, one-pot synthesis and two-pot synthesis. One-pot coating synthesis on the CdSe QDs is a new routine which is achieved in a single step including the formation of CdSe QDs. Before the QDs were separated, the mixture was cooled to ~200 °C. Then, after being kept three minutes at this temperature a solution containing 250 µl hexamethyldisllathiane ($(TMS)_2S$) and 1 ml diethylzinc ($Zn(Et)_2$) premixed in 2 ml TOP was gradually injected into the solution over a minute. Due to the desired thickness of ZnS layer, the amount of $(TMS)_2S$ and ($Zn(Et)_2$) accordingly vary. The reaction mixture was kept at 180 °C and stirred for one hour. The solution was cooled to room temperature and the resulting sample of CdSe/ZnS QDs was washed three times with methanol and chloroform before being redissolved in chloroform.

Two-pot synthesis divides the CdSe synthesis and coating of ZnS into two steps. After the CdSe QDs were formed (as color turn to desired color), the mixture was cooled down and dissolved in chloroform. After being washed with methanol and chloroform three times, CdSe QDs were redissolved in chloroform. The solution was then mixed with 3 g TOPO in a flask. The chloroform was bulbed away with nitrogen under stirring. Heating mantle was installed. A solution containing 250 µl hexamethyldisllathiane ($(TMS)_2S$) and 1 ml diethylzinc ($Zn(Et)_2$) premixed in 2 ml TOP was gradually injected into the solution over a minute when the mixture was heated up to ~200 °C. The reaction mixture was then kept at 180 °C and stirred for one hour before it was washed and redissolved in chloroform.

2.3 Surface Modification of Quantum Dots with Thiol Ligands

The QDs were synthesized in organic surfactant TOPO. As a result, the CdSe and CdSe/ZnS QDs are capped with TOPO ligands and they can only dissolve in organic solvent such as chloroform, hexane, but not some polar solvents such as alcohol and water. [2] In order to make them water-soluble, hydrophilic ligands with thiol (-SH) groups were applied to exchange with the surfactant groups. Not much is revealed so far regarding the nature and chemical properties of the binding between nanocrystals and thiol ligands. A possible mechanism is thiol groups bind to the metals on the crystal surface at the expense of decreasing the nanoparticle's size. The thiol groups have been the most utilized ligands for modifying semiconductor nanocrystals. [15,16,20,25] Aldana et al. (25) successfully capped CdSe QDs with a series of ligands including mercaptoacetic acid, mercaptobenaoic acid, mercaptopropionic acid, 11-mercaptoundecanoic acid, dihydrolipoic acid, and 1,4-dithio-D, L-threitol. In Gerion's report [15], a biocompatible water-soluble silica layer was coated on CdSe/ZnS QDs by using multiple thiol ligands. Guo [26] successfully enclosed QDs in dendron boxes via dendrimer bridging. Those semiconductor box nanocrystals exhibit biocompatibility and exceptional thermal stability.

To enable water-solubility, we used a method reported by Peng et al. [25] about 5 ml ~ 1μM CdSe/ZnS quantum dots chloroform solution was loaded into a 250 ml flask and heated up to 60 °C. 2 ml mercaptoacetic acid was injected into the flask. The whole mixture was refluxed at 60 °C for 16 hours under stirring. The precipitation was

separated from the chloroform by centrifugation. The QDs solution was washed with methanol and chloroform twice and dissolved in water at the end.

2.4 Oxygen Sensitivity of Water-Soluble Quantum Dots

About 10 mg thiol-coated CdSe quantum dots were dissolved in 1.5 ml of de-ionized water. The solution was transferred into a quartz cuvette. Then the solution was bubbled with a light flow of oxygen, nitrogen and air in turn for 15 minutes under dark respectively. Between every two kinds of gases, fluorescence emission was recorded with Quanta Master PTI fluoremeter under same operation conditions. Then same procedure was repeated from oxygen to air, nitrogen. (all under room temperature)

2.5 Synthesis of Luminescent/Magnetic Particles

The coupling between the luminescent CdSe/ZnS QDs and the magnetic beads was based on thiol chemistry. Thiol groups form stable bonds with metals on the surface of QDs like cadmium and zinc [5,19,20,26]. The magnetic particles were purchased from Indicia, France and they were modified free thiol and carboxylic groups. However, the coupling reaction between the QDs and magnetic beads presented a difficulty since the trioctylphosphine oxide (TOPO) capped CdSe/ZnS QDs were dissolved in chloroform while the polymer (DMSA)-coated magnetic beads were dispersed in water. We found that running the coupling reaction in a 10:5:1 mixture of chloroform:methanol:water yielded the best nanocomposite particles with minimal aggregation. To carry out the

coupling reaction we first transferred 1 ml of 1 μM CdSe/ZnS QDs into a 5 ml vial. Then we added 500 μl methanol to the solution. This was followed by the slow injection of 100 μl 0.1 μM magnetic beads water suspension to the solution under sonication and vigorous stirring. Under these reaction conditions the molar ratio between the QDs and the magnetic particles was 100:1. The excess of QDs was imperative to preventing aggregation of the magnetic beads. Under vigorous stirring the aqueous and organic phases formed an even suspension. The suspension was stirred for 1 hour to form the nanocomposite particles. The magnetic/luminescent were then separated from the solution by using a permanent magnet (Average cross sectional force density 16.6 T^2/m) and washed several times with methanol. The sample was vortexed briefly and sonicated for 15 minutes to prevent aggregation.

In order to make the magnetic/luminescent particles biocompatible, the magnetic/luminescent suspension was transferred into a 250 ml flask. After the flask was heated to 60 °C under magnetic stirring, 200 μl mercaptoacetic acid was injected. The mixture was refluxed for 1 hour at 60 °C under stirring. Then the magnetic/luminescent particles were separated with a magnet and washed twice with 5 ml DI water. Before they were resuspended in DI water, the particles were briefly vortexed and sonicated for 15 minutes to prevent aggregation. The suspension was stored in the dark.

2.6 Protocol of EDAC Coupling

Reagents:

1. Carboxyl-Modified magnetic/luminescent particles (~10nm)

2. PBS buffer (PH=7.4)

3. 1-Ethyl-3- (3-dimethylaminopropyl) carbodiimide (EDAC)

4. Antidoby (Mouse anticyclin E)

Procedures:

1. Separate the particles with magnetic and wash them with PBS buffer twice. Then resuspend the particles in 1 ml PBS (PH=7.4) buffer (~0.1 μM)
2. Briefly vortex and 15 minutes sonication are used to prevent aggregation
3. 10 μl mouse anti-cyclin E antibody solution is added into the magnetic/luminescent particle suspension
4. 100 mg EDAC coupling reagent is added into the mixture
5. Gently shake the mixture for 30 minutes. Then the antibody bound luminescent/ magnetic particles (QMAb) are separated from the suspension with a magnet.
6. Wash the QMAb particles with 2 ml PBS buffer twice. Then resuspend the QMAb particles in PBS buffer

2.7 Characterization

Absorption Spectra: Absorption spectra of free QDs in solution and their nanoassemblies were obtained using a Varian UV-VIS-NIR spectrophotometer system, model CARY 500 Scan.

Fluorescence Emission Spectra: Emission spectra of free QDs solution and their nanoassemblies were taken in a quartz cuvette using a PTI Quanta Master luminescence spectrometer equipped with a 75 W xenon short-arc lamp as a light source.

Measurement of Quantum Yield: The quantum yield was measured using PTI Quanta Master luminescence spectrometer and Varian UV-VIS-NIR spectrophotometer by comparing the integrated emission intensity of QDs with a standard (Rohdamine B). Using the data derived from luminescence and the absorption spectra, the quantum yield was calculated following:

$$\mathbf{QY=\{(1-T_{ST})/(1-T_X)\}(\Delta\Phi_X/\Delta\Phi_{ST})q_{ST}}\ [3]$$

Where T_{ST} and T_X are the transmittances at 400 nm fro the standard and the sample, respectively, and q_{ST} is the quantum yield of standard (Rohdamine B 90%, Sigma). The terms $\Delta\Phi_X$ and $\Delta\Phi_{ST}$ give the integrated emitted photon flux (photons s^{-1}) for the sample and the standard respectively, upon 400 nm excitation. The accuracy of the method is estimated to be ±10%.

Microscopy: Luminescence images of QDs aggregates and QDs nanoassemblies were obtained using a digital luminescence imaging microscopy system. (Figure 2.1) The system consists of an inverted fluorescence microscope (Olympus IX70) equipped with a 100 W mercury lamp as a light source. The fluorescence images were collected using a 40× microscope objective with NA = 0.9. A filter cube containing a 330-385-nm band-pass excitation filter, a 400-nm dichroic mirror, and a 420-nm long-pass emission filter was used to ensure spectral imaging purity. A high-performance ICCD camera (Princeton Instruments, model BH2RFLT3) was employed for digital imaging of the CdS QDs. A

PC microcomputer was employed for data acquisition. The Roper Scientific software WinView/32 was used for image analysis.

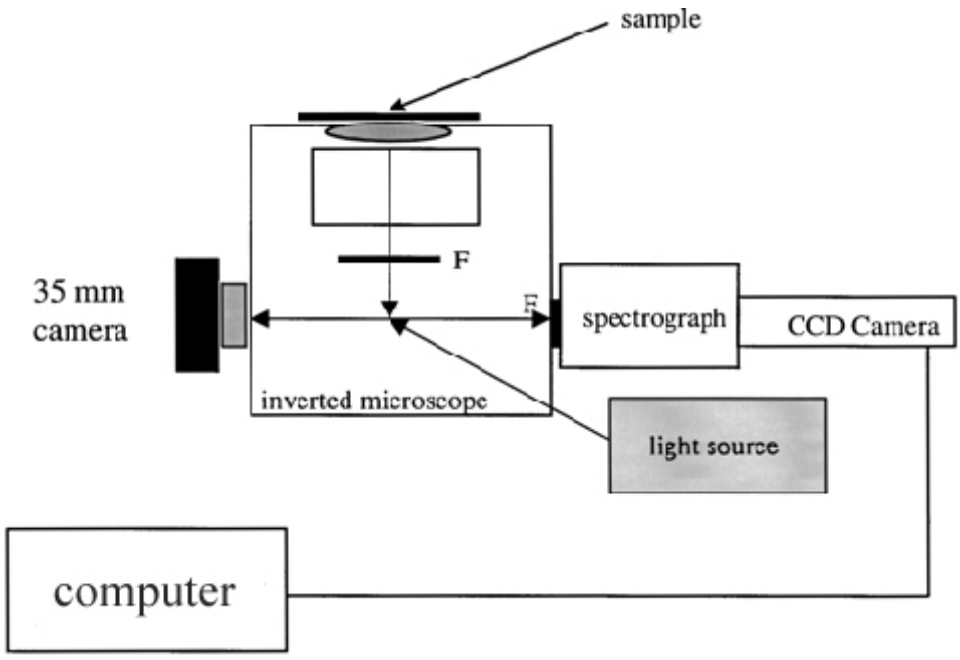

Figure 2.1 Digital fluorescence imaging microscopy system [41]

Transmission Electron Microscopy: The size and morphology of free QDs and their nanoassemblies were characterized using a JEOL 2010 electron microscope. EDS analysis was taken accompanying with the TEM image.

2.8 Biological Experiments

2.8.1. Breast Cancer Cells (MCF-7) Preparation

1. Frozen breast cancer cells MCF-7 were purchased from the American Tissue Culture Collection (ATCC).

2. The cells thawed under room temperature before incubating.

3. The breast cancer cells were raised in an incubator under 37 ^{o}C 5% CO_2 for at least two days before experiment in serum medium. The cells are cultured composed of 500 ml DMEM (Dulbecco's Modified Eagle's Medium), 50 ml FBS (Fetal Bovine Serum), 5 ml Antibiotic-antimycotic, 20 ml L-glutamine, 5 ml Sodium Pyruvate, 5 ml Non-Essential Amino Acids.

4. Remove medium

5. Add 5 ml trypsin

6. Incubate under 37 ^{o}C 5% CO_2 for 5-10 minutes in incubator

7. Collect cell suspension to a centrifuge test tube

8. Centrifuge 10 minutes at 1700 RPM

9. Remove Trypsin

10. Wash the cells with 5 ml PBS buffer (PH 7.4) twice

11. Resuspend cells in PBS buffer (PH 7.4)

2.8.2 Cell Labeling

Separation from suspension:

1. Transfer 100 μl QMAb particle suspension (DI water) into a 1 ml test tube.

2. 500 μl breast cancer cell suspension (10,000/ml in PBS buffer) was transferred into the test tube.

3. Gently shake the mixture for about 15 minutes.

4. Apply a magnet to separate the cells from the liquid and remove the liquid from the test tube

5. Wash the cells with PBS buffer (PH=7.4) twice with the magnet.

6. Observe the cells under fluorescence microscope.

Separation from red blood cells

1. Transfer 100 μl QMAb particle suspension (DI water) into a 1 ml test tube.

2. 500 μl breast cancer cell suspension (10,000/ml in PBS buffer) and 500 μl red blood cell suspension (10,000/ml) was transferred into the test tube.

3. Gently shake the mixture for about 15 minutes.

4. Apply a magnet and remove the liquid from the test tube

5. Wash the cells with PBS buffer (PH=7.4) twice with the magnet.

6. Observe the cells under fluorescence microscope

CHAPTER 3: RESULTS AND DISCUSSIONS

3.1 Synthesis of CdSe and CdSe/ZnS Quantum Dots

A typical absorption and fluorescence spectra of CdSe Quantum Dots (QDs) (Figure 3.2) can show us that it has sharp and narrow fluorescence emission. The half-width is around 30 nm which is much narrower than usual organic dyes. It also has a very wide excitation range. For QDs emission at 550 nm, its excitation can range from 400 nm to 530 nm. Compared to organic dyes, it is another advantage that different color QDs can be excited at the same time with one single excitation source. The tunable size and color of QDs has offered a possibility to use different color QDs as sensors which can all be observed under one excitation in one experiment.

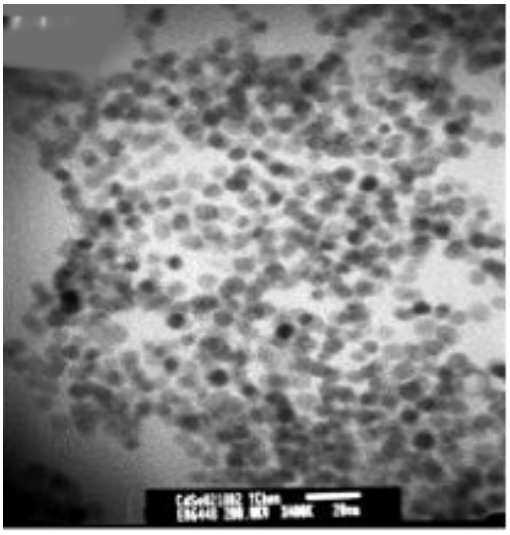

Figure 3.1 TEM image of CdSe/ZnS QDs. The scale bar is 20 nm. [62]

Semiconductor nanocrystals synthesized by means of colloidal chemistry techniques provide a successful realization of the strong quantum confinement [1,63] with an advantage of continuous tunability of the electronic and optical properties by changing the physical size of the nanocrystals. Introducing hexadecylamine as a cosurfactant to the TOPO-TOP stabilizing mixture narrows the size distribution of CdSe nanocrystals during their growth and allows a considerable improvement of their photoluminescence (PL) properties. The emission efficiency, spectrum, and time evolution of quantum dots are strongly affected by the surface. A better surface structure can provide higher stability, higher quantum yield and longer lifetime. The function of ZnS layer is to passivate the surface of CdSe QDs (Figure 3.3). The QDs lose a large portion of efficiency mostly because of electron leaking [21] which is resulted from the surface defects of CdSe QDs. In order to improve the quantum yield, a larger band gap material (ZnS, ZnSe, etc) is usually used to passivate the surface. As shown in Figure 3.6, a leaking electron needs to cross a band gap barrier which is higher than CdSe before escaping from quantum bulk. So the ZnS band gap barrier will block a large amount of electrons which used to escape from interior crystal of the QDs and end up non-radiative decay. The passivation layer increases the quantum yield of QDs dramatically from 10-15% to 50% (Figure 3.8) in two-pot synthesis. [22] A one-pot synthesis method could increase the quantum yield up to 100%. [23,24]

Upon comparison of one-pot and two-pot synthesis method, the CdSe/ZnS QDs synthesized with one-pot showed extremely high quantum yield reaching 100%. We even can see the shining fluorescence under room light. The reason for dramatic increase of quantum yield in comparison to two-pot synthesis is probably ZnS forms right after CdSe

crystal growth's ending so that there are less surface defects between CdSe and ZnS. In case of two-pot synthesis, before ZnS coating the CdSe crystal is already formed and the surface is capped by TOPO/TOP. In the second pot (ZnS coating), the formation of ZnS layer could enclose some TOPO/TOP which forms a gap between CdSe and ZnS ending up defects. The stability of CdSe QDs was also improved by ZnS coating.

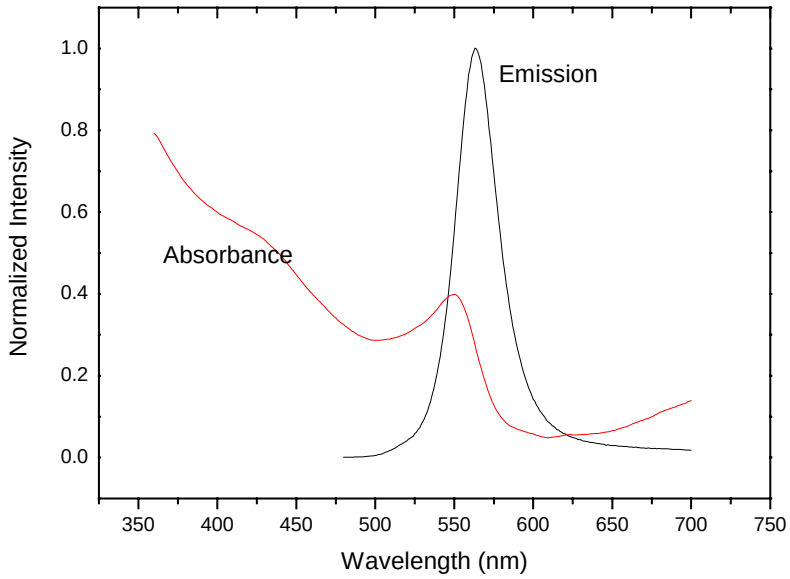

Figure 3.2 Typical absorption and fluorescence spectra of CdSe quantum dots room light.

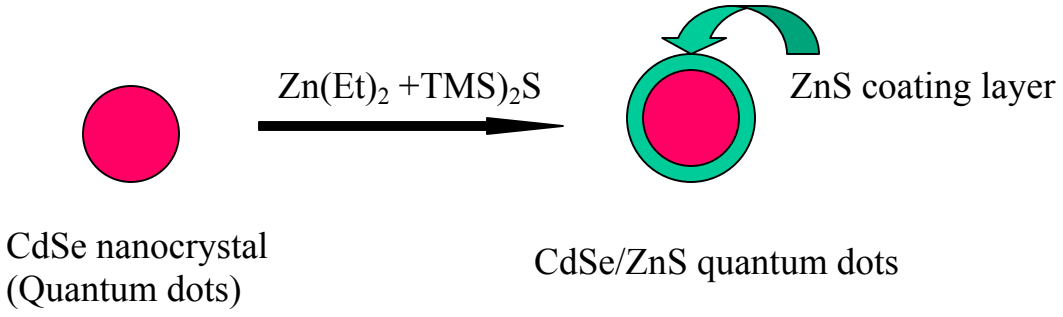

Figure 3.3 Schematic digram of ZnS coating on CdSe quantum dots

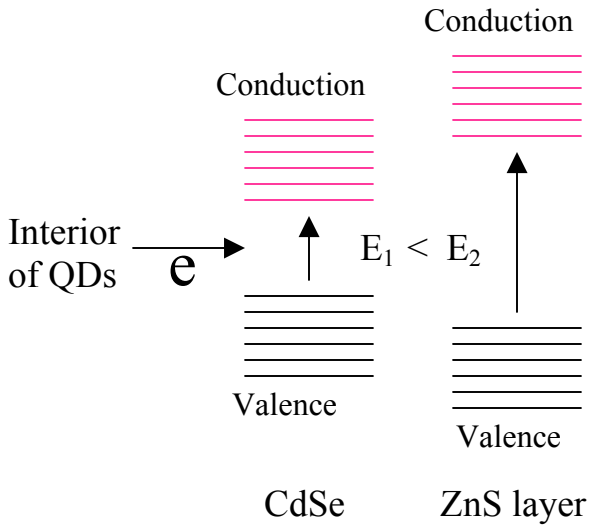

Figure 3.4 Schematic of ZnS coating as a band gap barrier

3. 2 Water Solubility of CdSe/ZnS Quantum Dots

To enable biocompatibility, it is imperative to convert hydrophobic surface ligands to hydrophilic ligands. The most utilized method is to exchange the surface groups with a compound that consists of both thiol groups and carboxylic groups such as mercaptoacetic acid (MAA), 4-mercaptobenzoic acid (MBA), 3-mercaptopropionic acid (MPA), 11-mercaptoundecanoic acid (MUA), Mercaptosuccinic acid (MSA). In our experiment, a method modified from Peng's [25] was applied. Experiments showed that thiols and metals on the surface of QDs form strong bonds at the expense of losing some stability. We used mercaptoacetic acid as the surfactant groups (Figure 3.5).

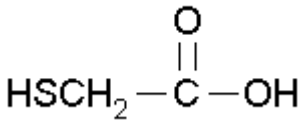

Figure 3.5 Mercaptoacetic acid

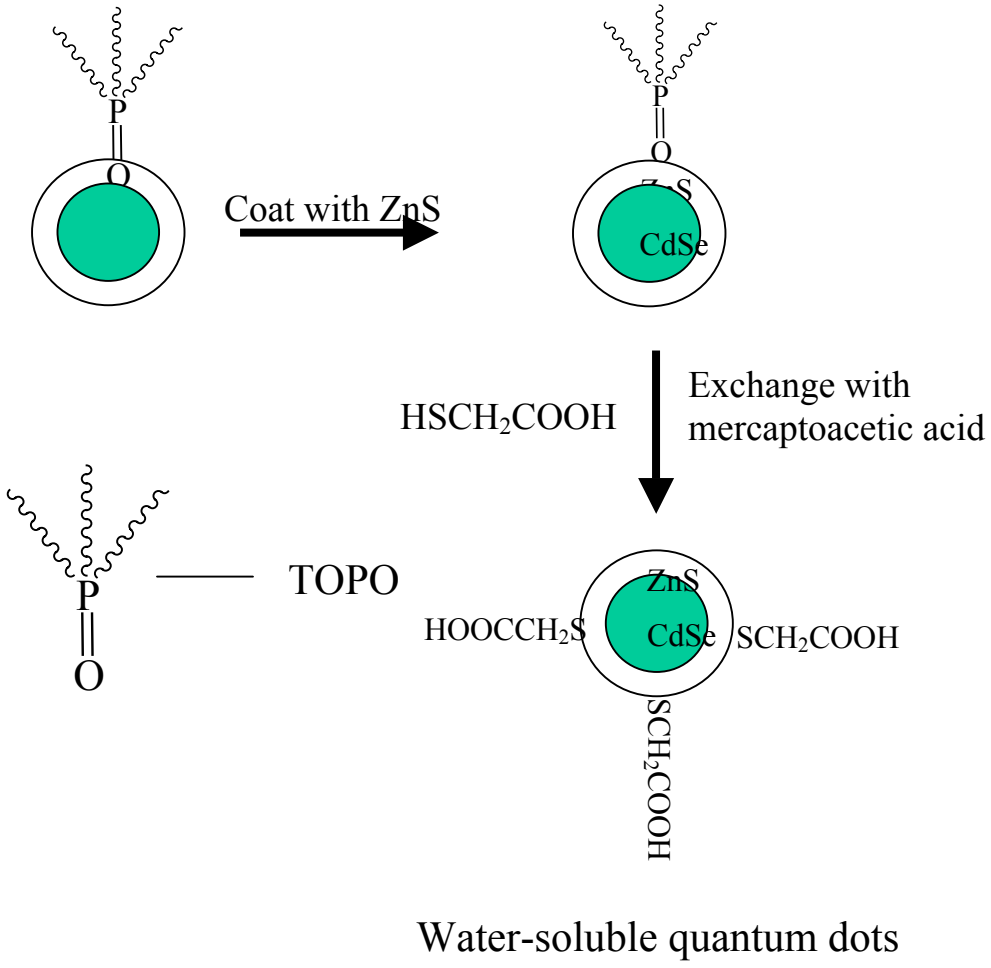

Figure 3.6 Schematic of pathways to passivate CdSe quantum dots and exchange with mercaptoacetic acid

Except the loss of stability, we also observed a blue shift and a loss of quantum yield as expected [25]. As we can see from Figure 3.7a, The CdSe quantum dots have a sharp and intense emission peak around 536 nm. After being coated with ZnS and thiol group, it still has intense emission as shown in Figure 3.7b and 3.6c with a little shift to 557 nm and 567 nm respectively. This red shift is due to the growth of Ostwald Ripening (which is the growth of some particles at the expense of other small particles) at high temperature [42]. There is also a drop of fluorescence emission. Considering the solutions

are in same concentration (assuming water as a solvent doesn't have a significant effect on fluorescence compared to chloroform), quantum yield of CdSe/ZnS-thiol QDs is lower compared to CdSe/ZnS (about 50% drop). A possible explanation for the phenomena might be that the stronger bond between the thiol and the metal atoms at the surface of QDs induces a redistribution of electronic density and an increase in confinement energy. [16] Further research is needed to clarify the cause of the drop of quantum efficiency and blue shift. However, the water-soluble CdSe/ZnS QDs still showed high quantum yield.

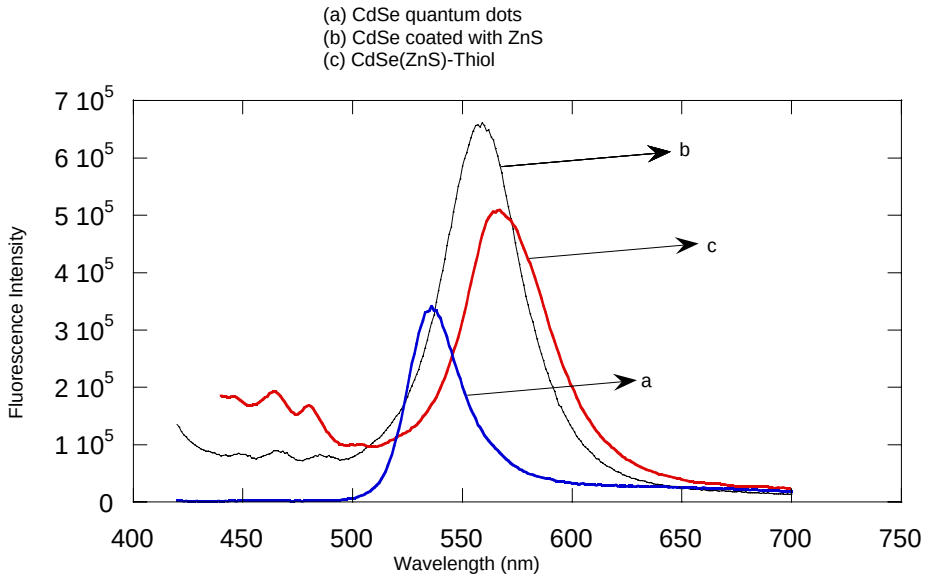

Figure 3.7 Emission spectra of (a) CdSe quantum dots in chloroform, (b) CdSe/ZnS chloroform, (c) CdSe/ZnS-Thiol in deionized water.

3.3 Oxygen Sensitivity of Water-Soluble CdSe/ZnS Quantum Dots

Intracellular oxygen concentration is a key indicator of numerous physiological and pathological processes in biological systems. In cells, excess oxygen leads to overproduction of the extremely reactive and unstable reactive oxygen species (ROS),

which oxidize lipids, carbohydrates, DNA, and proteins, altering their structure and function. [49,50] The determination of oxygen concentration is of particular importance in tumor cells since it may enable the prediction of the response of the tumor to radiation and chemotherapy. [51-53]

During the experiment, we found out that luminescence intensity of thiol-coated quantum dots is 4 times higher in nitrogenated solution than in oxygenated solution (Figure 3.8). This observation means oxygen is a strong quencher of CdSe/ZnS quantum dots. Therefore, there is a potential to apply CdSe/ZnS quantum dots as a probe to measure oxygen concentration in biological systems. The application of quantum dots as oxygen probe offers several advantages. First, high sensitivity because of the high luminescence of quantum dots and strong oxygen quenching; second, could be used to measure intracellular oxygen concentration due to the small size of quantum dots; third, the technique is minimally invasive, allowing measurement of live cells. [41] The limitation so far is that the fluorescence emission drops sharply almost to zero after one cycle of sensitivity test, which is due to the instability of thiol coated quantum dots. [25] The quantum dots precipitated out of the solution during the experiment. Not much is known regarding the nature and chemical properties of the binding between nonacrystals and their ligands. The most likely mechanism of emission quenching is due to irreversible photooxidation of the quantum dots. When this happens, the ligands are catalytically oxidized under UV light to form disulfides with CdSe nanocrystals acting as the photocatalysts. [25] Another possible reason is that there is only one thiol group for each ligand connected to the complex surface of quantum dots. The binding is fragile upon

oxidation of oxygen and the surface didn't form a perfect coating to prevent oxygen from

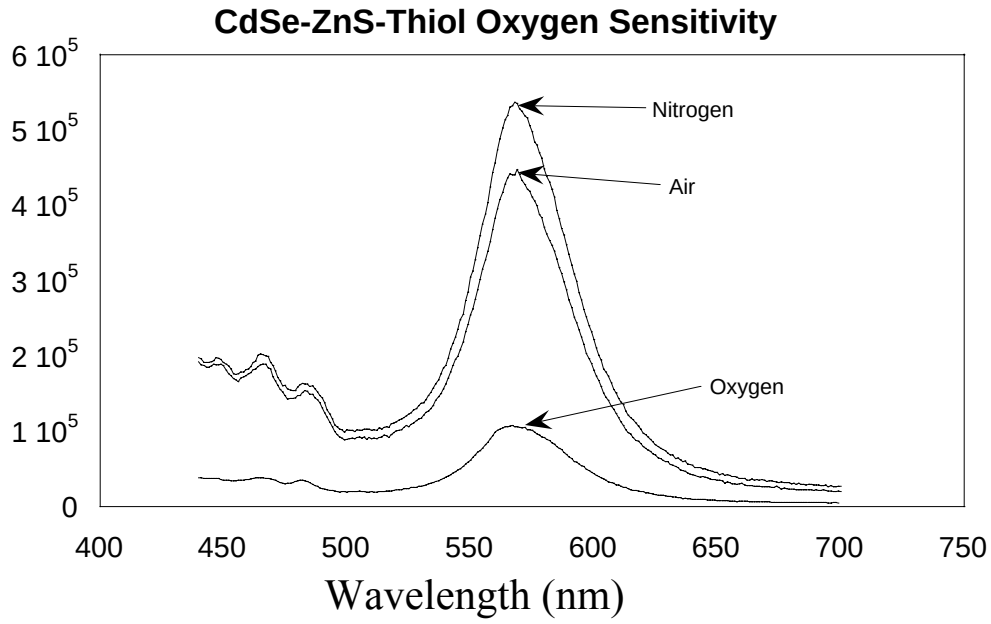

getting through the ligands.

Figure 3.8 Spectra of nitrogenated, oxygenated and air-saturated quantum dots water solution

As a result, thiol-coated CdSe/ZnS water-soluble quantum dots have strong visible emission. They could be used as oxygen probes in biological system due to the strong oxygen quenching. However, mercaptoacetic acid coated CdSe/ZnS quantum dots are not stable due to photooxidation and currently cannot be used to monitor oxygen dynamics. Further investigation may focus on stabilizing the water-soluble quantum dots in order to provide them with reversible oxygen sensitive properties. Multiple bonds or polymerization ligands have been tried as surfactants to functionalize QDs [15,43]. Results showed higher stability under same circumstances.

3.4 CdSe/ZnS Quantum Dots-Magnetic Beads Luminescent/Magnetic Particles

A new type of nanocomposite particles, CdSe/ZnS Quantum Dots-Magnetic Beads Core-Shell luminescent/magnetic particles, was synthesized through thiol binding. Polymer coated γ-Fe_2O_3 superparamagnetic magnetic beads were purchased from Indicia Biotech, France. A cartoon diagram is shown in Figure 3.9. The nanometric γ-Fe_2O_3 magnetic particles were made by coating Ferrofluid with dimercaptosuccinic acid (DMSA). The goal of DMSA coating was to stabilize and functionalize the particles. The surface of the Ferrofluid was covered with free thiol (SH) and carboxyl (COOH) residues (3:20 thiol to COOH ratio) to enable covalent coupling of various ligands to the magnetic particles [17]. The nanocomposites showed both luminescent and magnetic properties. A schematic of the particle formation is shown in Figure 3.9. The luminescent/magnetic particles can be further modified with mercaptoacetic acid to acquire water solubility.

A TEM image (Figure 3.10a) of the polymer coated particles shows that their magnetic core averages 10 ± 15% nm in diameter. The hydrodynamic diameter of the luminescent/magnetic particles that include the polymer layer was found to be around 20 ± 10% nm based on dynamic light scattering measurements. The particles were fully miscible in aqueous solution and no aggregation was observed.

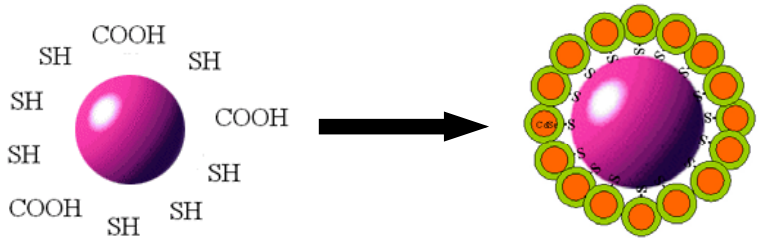

Figure 3.9 Thiol and carboxy modified γ-Fe_2O_3 beads are reacted with CdSe/ZnS QDs to form the luminescent/magnetic nanocomposite particles.

A representative TEM image of the nanocomposite particles is shown in Figure 3.10b. The particles average 20 nm in diameter with a size distribution of about 15% and show minimal or no aggregation. Assuming the magnetic beads are fully covered with QDs, the maximum number of QDs per magnetic bead could be estimated based on the following equation:

$$N = 2\pi (R_{Fe} + R_{QD})^2 / \sqrt{3}\, R_{QD}^2$$

R_{Fe} is the radius of the magnetic beads and R_{QD} is the radius of the smaller QDs. This estimated expression is derived by dividing the surface area covered by the small QDs on the larger iron oxide particle by the area covered by a single QD on the iron oxide particle surface. The calculation assumes close packing of QDs on the magnetic particle surface and takes into consideration the gaps between the QDs. For example, for a magnetic particle diameter of 10 nm, the maximum number of QDs increases from 45 to 133 when the QDs diameter decreases from 4 to 2 nm. A high resolution TEM image of an individual magnetic bead coated with CdSe/ZnS QDs is shown in Figure 3.10c. Gaps between the QDs can be seen, which indicates imperfect coating. It also implies that the number of QDs per magnetic particle would be lower than the upper theoretical limit.

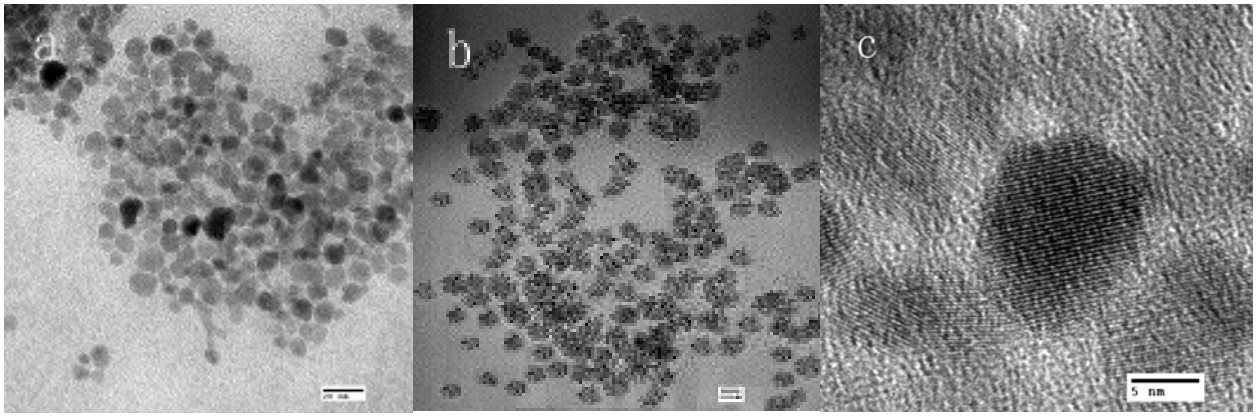

Figure 3.10 a) A TEM image of magnetic beads (γ-Fe_2O_3) with polymer coating, the scale bar is 20 nm; b) A TEM image of QDs magnetic beads core-shell nanoparticles. The scale bar is 20 nm. c) A high resolution TEM image of a single magnetic bead coated with quantum dots. The scale bar is 5 nm.

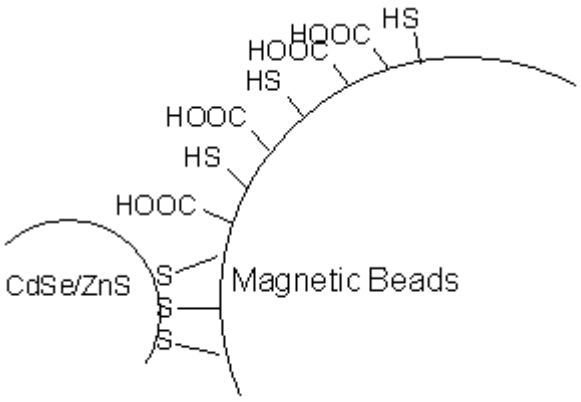

Figure 3.11 Proposed formation mechanism of magnetic beads (γ-Fe_2O_3) quantum dots CdSe/ZnS core-shell nanoparticles. (TOPO---trioctylphosphine oxide)

Figure 3.11 shows the formation mechanism of the luminescent/magnetic particles. The number of thiol binding between a single quantum dot and magnetic bead might be different respect to the size and shape of the magnetic particle. An Energy Dispersed Spectrum (EDS) of the nanocomposite particles is in Figure 3.12. The Cu peaks result from the sample grids. Spectral peaks that originate from the QDs coating of the magnetic beads indicate the presence of Cd, Se, Zn, and S on the surface of the iron

oxide particles. The relatively high Zn and S peaks could indicate the presence of multiple layers of ZnS on the surface of the CdSe QDs [23,44,45].

Luminescence microscope images (400× magnification) of the nanocomposite particles coated with ~3 and ~5 nm CdSe/ZnS QDs are shown in Figures 3.13a and 3.13b, respectively. A large signal-to-background ratio of over 100 is observed in these digital images. No micrometric clusters of nanocomposite particles are seen.

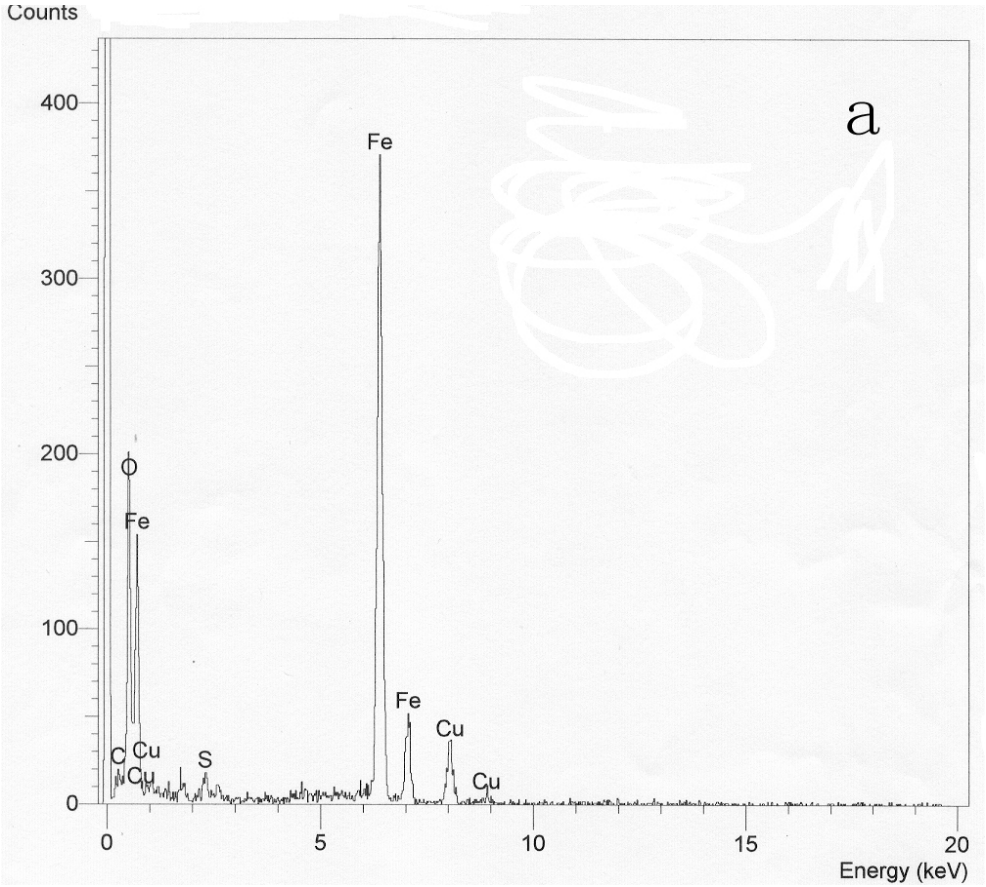

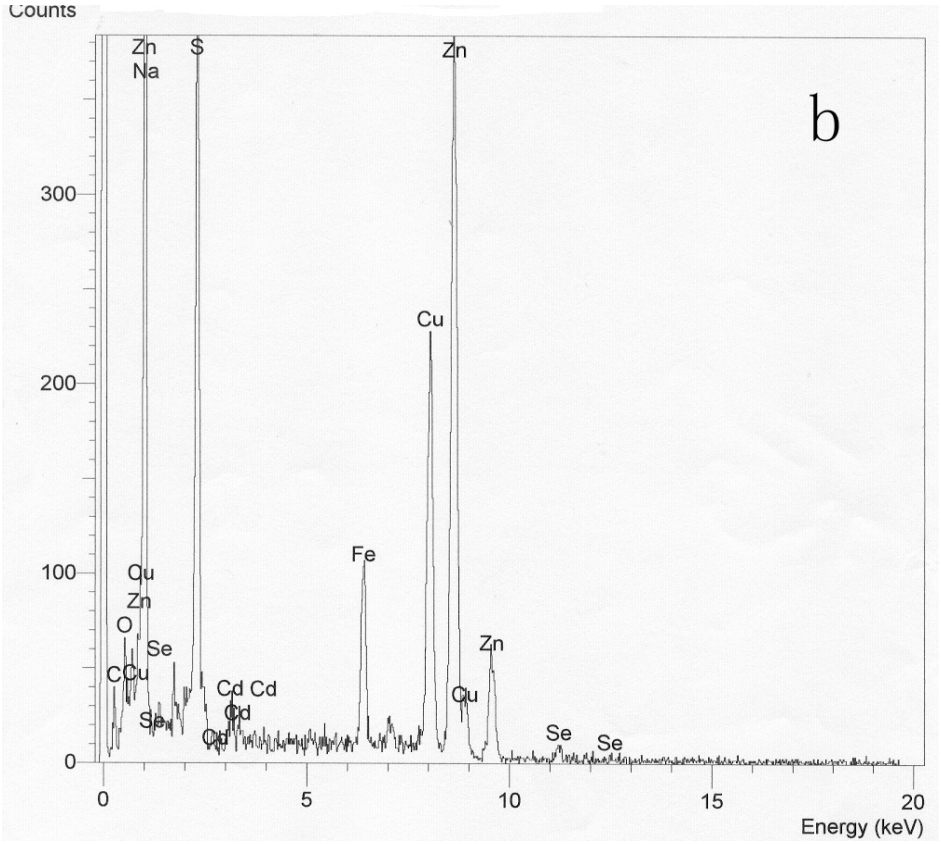

Figure 3.12 EDS (Energy Disperse Spectroscopy) spectrum. a) Blank magnetic beads; b) luminescent/magnetic core-shell particles.

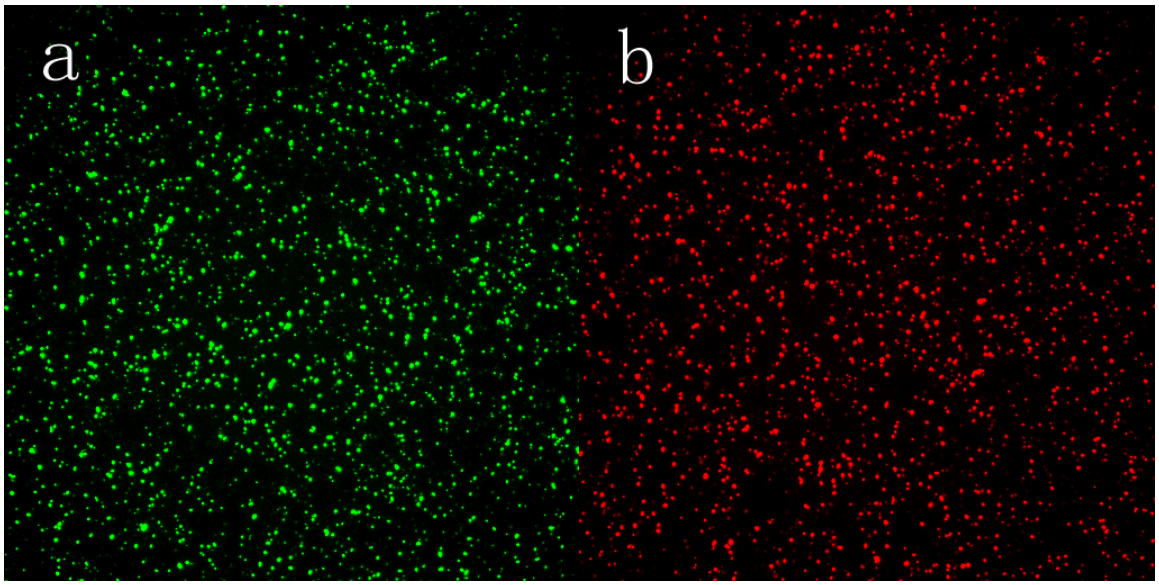

Figure 3.13 Digital fluorescence microscope images (40X) of magnetic beads coated with a) 3 nm and b) 5 nm CdSe/ZnS QDs

Luminescence spectra of CdSe/ZnS QDs in chloroform and CdSe/ZnS QDs- γ-Fe_2O_3 luminescent/magnetic particles in aqueous solution are shown in Figure 3.14. A slight blue shift is observed which could be attributed to a change in surface states of the quantum dots due to the immobilization. The emission quantum yield of the nanocomposite particles was found to be around 0.18, which is 3 times lower than the emission quantum yield of CdSe/ZnS QDs in chloroform (0.61). The drop in emission quantum yield is attributed to the solvent change and to possible changes in electronic density on the surface of the QDs due to the immobilization. While the ZnS capping passivates the surface of the CdSe QDs the capping is not perfect allowing electrons to leak to the surface of the QDs. These free electrons could interact with the polymer coated magnetic core particle and this interaction, which in turn could cause a decrease in the emission quantum yield. Leakage of electrons from QDs has been previously observed when the surface of CdSe/ZnS QDs was modified with mercaptoacetic acid (or MPA, MUA) [16]. It was shown that the result of this leakage is a decrease in the emission quantum yield and a blue shift in the emission spectrum of the modified QDs. It should be noted however that the width of the emission peak of the QDs is not affected by the coupling of QDs to the polymer coated magnetic nanoparticles.

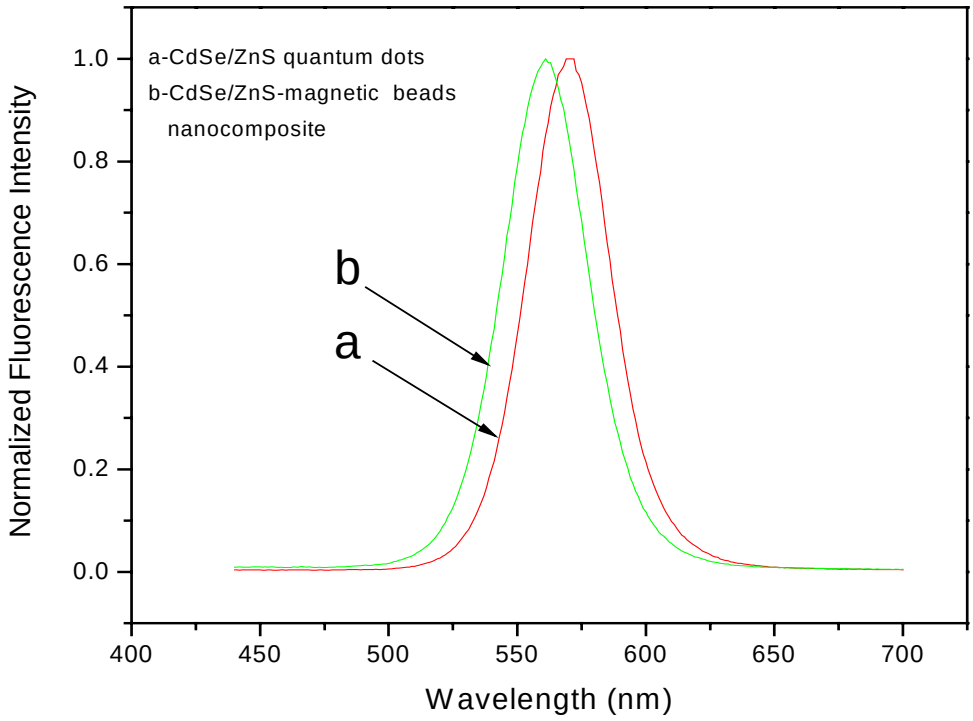

Figure 3.14 Fluorescence emission spectra. a(red): CdSe/ZnS QDs in chloroform; b (green): magnetic beads CdSe/ZnS quantum dots core-shell nanoparticles in water.

Luminescence lifetime of the luminescent/magnetic nanoparticles showed an excited-state lifetime of 65 ± 5 ns. The excited-state lifetime of CdSe/ZnS nanoparticles was 27 ± 3 ns. This excited-state lifetime of the CdSe/ZnS QDs was in agreement with previous studies. [48] It should be noted that the lifetime measurements yielded only approximate values since the fluorescence decay times exhibited significant variations from exponential decay curves. Nevertheless, the clear increase in excited state lifetime could be attributed to quenching interactions between the magnetic nanoparticles and the luminescent QDs or between the close packed QDs.

3.5 Biological Application

3.5.1 Breast Cancer Cells Labeling

To demonstrate their utility we immobilized anticycline E antibodies on their surface and used the antibody coated particles to separate MCF-7 breast cancer cells from serum solutions.

In order to apply the luminescent/magnetic particles for magnetic separation of cells followed by luminescence detection, they were first modified with carboxylic functional groups. 2 ml 0.1 μM luminescent/magnetic particle suspension in methanol was transferred into a 250 ml flask, which was heated to 60 °C under stirring. Then, 200μl mercaptoacetic acid (Sigma) was injected into the flask. The reaction took 1 hour to complete. The carboxyl-modified luminescent/magnetic particles were washed 3 times with DI water by magnetic decantation and were finally dispersed in 2 ml DI water and briefly vortexed to prevent aggregation. As expected, the modified luminescent/magnetic particles were highly water-soluble and also maintained their luminescence properties [15,25]. Mouse anticycline E antibody (Zymed) molecules were attached to the luminescent/magnetic particles through EDAC (1-ethyl-3- (3-dimethylaminopropyl) carbodiimide) coupling as shown in Figure 3.15:

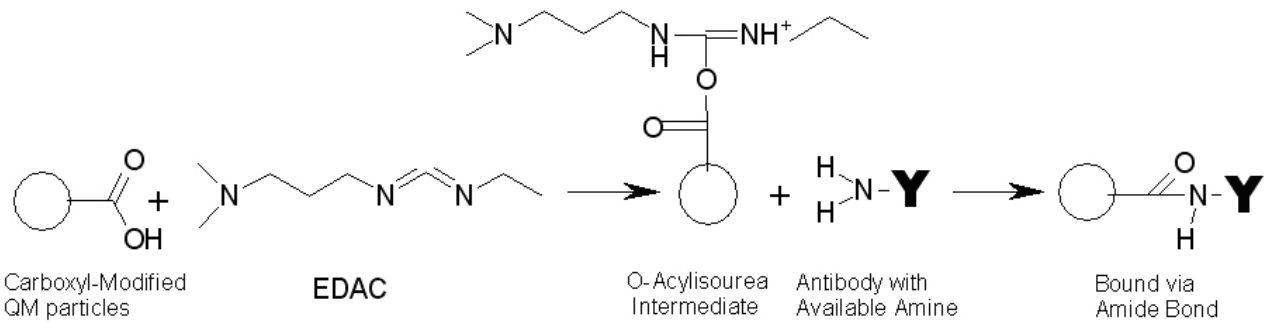

Figure 3.15 Schematic of covalent attachment of anti cycline E to the luminescent/magnetic particles using EDAC coupling chemistry

In our experiment, we used anti cycline E antibody. Information from Zymed tells us the EDAC coupling will not affect the binding activity of antibody since most amino groups ($-NH_2$) are not on the active site. Anticycline E antibodies bind specifically to cycline, a protein which is specifically expressed on the surface of breast cancer cells

10 μl Mouse anti cycline E antibody solution were added into 1 ml ~0.1 μM luminescent/magnetic particle suspension in a phosphate buffer (PBS) solution at pH 7.4. Then 100 mg EDAC coupling reagent were added into the mixture. The mixture was gently shaken for 1 hour and the antibody modified luminescent/magnetic particles were then separated and washed using magnetic decantation. The antibody modified luminescent/magnetic particles were resuspended in 1 ml PBS buffer solution at pH 7.4. The use of EDAC coupling enabled the covalent attachment of the antibodies to the carboxyl-modified luminescent/magnetic particles without substantially damaging the active site of the antibodies. [46]

To demonstrate the separation capability of the particles, a preliminary experiment was done. We incubated a sample of 200 μl anti cycline E modified luminescent/magnetic particles with a 1 ml MCF-7 breast cancer cell suspension containing 10,000 cells/ml. Following 15 minutes incubation at room temperature under gentle shaking the cells were separated from the suspension using a permanent magnet. The cells were washed twice with a phosphate buffer solution using magnetic decantation and observed using digital fluorescence imaging microscopy. Transmission and fluorescence microscope images of the MCF-7 cells labeled with the anti cycline E modified luminescent/magnetic are shown in Figure 3.16. The cells were successfully pulled to the magnet, which meant that they were successfully bonded to anti cycline E coated luminescent/magnetic particles. Control experiments with luminescent/magnetic particles that were not labeled with anti cycline E showed only negligible non-specific binding of luminescent/magnetic particles to MCF-7 cells. While free luminescent/magnetic particles were also pulled to the magnet they could be easily distinguished from cells because of the 3-4 orders of magnitude size difference between the luminescent/magnetic particles and the MCF-7 cells. The cell separation studies described here made use of a single antibody and luminescent quantum dots of a single emission color. It is possible to use luminescent/magnetic particles of different emission colors and different antibodies where the emission color would code for a specific antibody. A typical microscope image is shown in Figure 3.16. Compared to the transmission image, the cells labeled with green QDs were easily seen. Strong emission of QDs gives the image a high resolution of cells. Control experiment with luminescent/magnetic particles without antibodies turned out to be negative. This would

enable the determination of multiple antigens on the cell surface, which has the potential to increase the specificity of cancer diagnosis and staging.

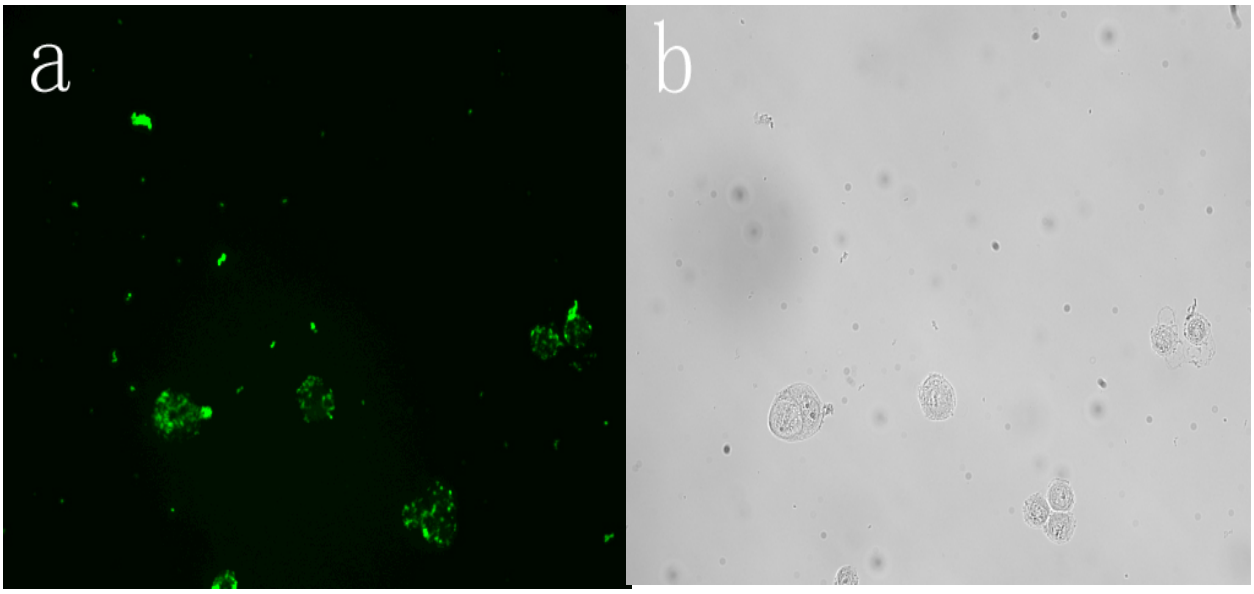

Figure 3.16 Fluorescence microscope image (40X) of breast cancer cells (MCF-7) with attached luminescent/magnetic particles. a) MCF-7 with green QDs luminescent/magnetic; b) Transmission image of (a).

3.5.2 Cells Separation

To further prove the cell separation of specific antibody-antigen binding instead of nonspecific binding we introduced red blood cells in the experiment. MCF-7 breast cancer cells are 1-2 times bigger than red blood cells. As shown in Figure 3.17, it is very easy to tell the difference between breast cancer cells and red blood cells under the microscope from their size and shape.

Control experiments proved there was no specific binding between luminescent/magnetic particles and red blood cells. The non-specific binding between luminescent/magnetic particles with anti cycline E antibodies and red blood cells was

neglectable. There was no aggregation between breast cancer cells and red blood cells in water or in PBS buffer (PH=7.4) in premixed suspensions.

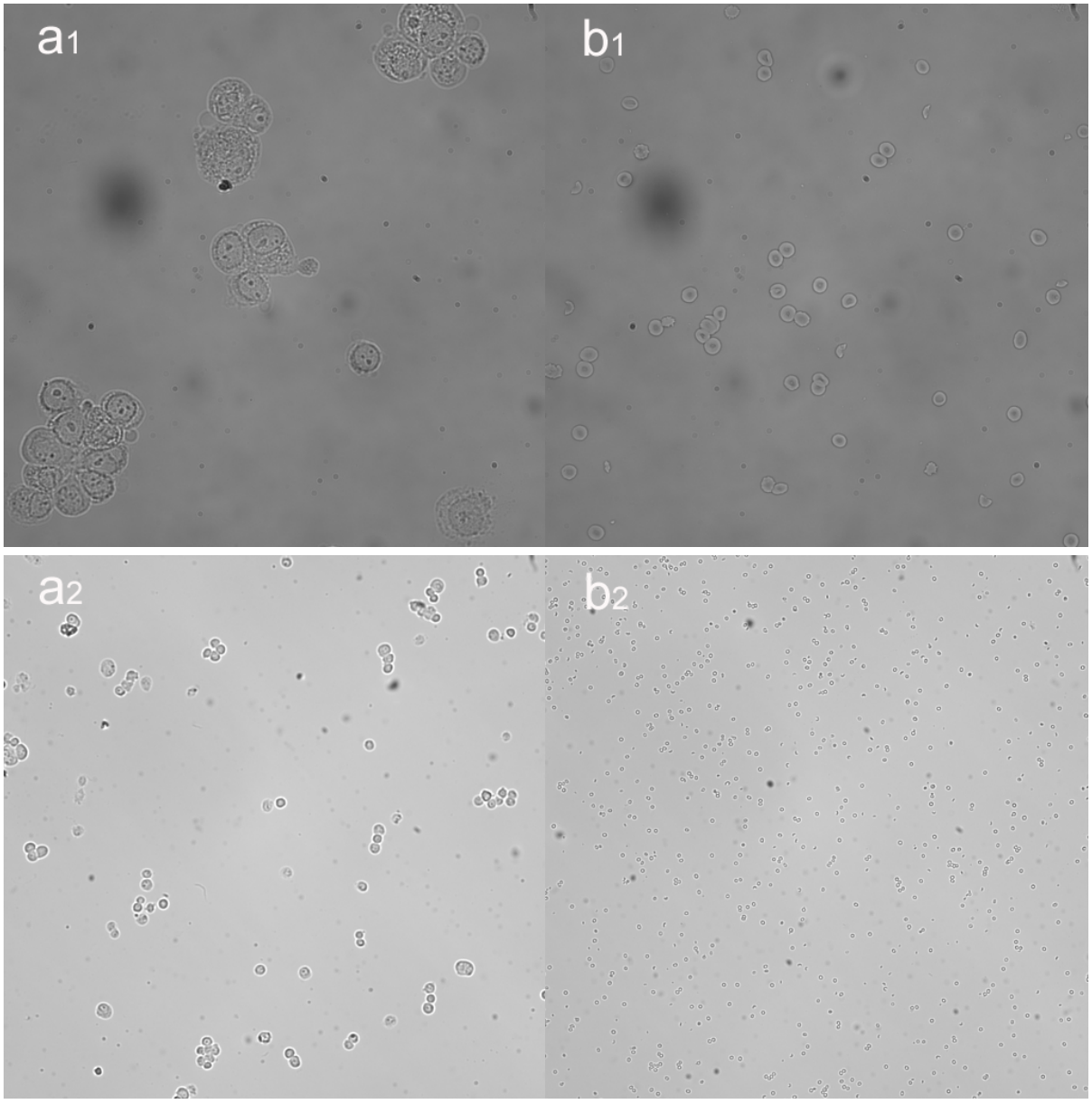

.

Figure 3.17 a1: high magnification (40X) of MCF-7 breast cancer cells; a2: low magnification (10X) of MCF-7 breast cancer cells; b1: high magnification (40X) of red blood cells; b2: low magnification (10X) of red blood cells. (above are all transmission images)

The experiment was performed in a suspension of same concentration of MCF-7 breast cancer cells and red blood cells. The mixture of anticycline E modified luminescent/magnetic particles and cells were gently shaken for 15 minutes. Then, the breast cancer cells were pulled out from the mixture through magnetic separation while red blood cells were left out in the suspension and later washed away with PBS buffer. Breast cancer cells were collected after separation with a magnet and washed. A 100 times magnification of fluorescence image of the cells is shown in Figure 3.18. Due to the strong emission of the particles, the breast cancer cells can be easily observed by fluorescence imaging microscopy. From the shape and size we can see that most particles were bound to breast cancer cells. No red blood cells were observed in the transmission and fluorescence images. In the suspension large quantity of red blood cells were observed while no breast cancer cells were observed.

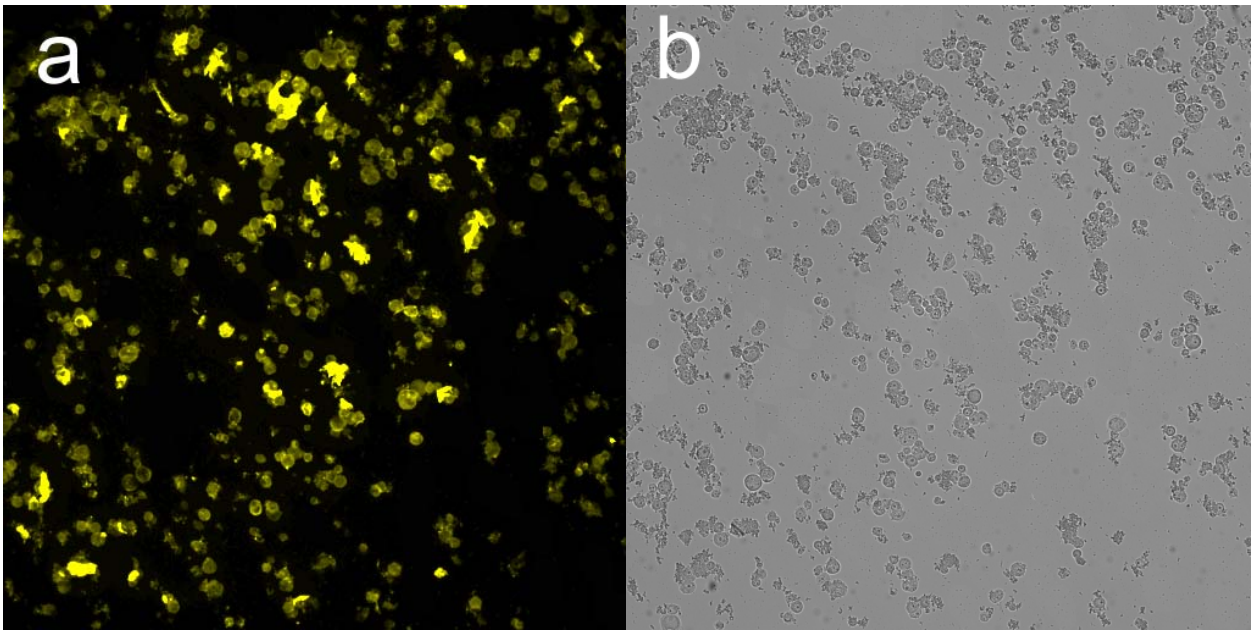

Figure 3.18 10 X Fluorescence (a) and transmission microscopy images of anti cycline E modified luminescent/magnetic particles attached to breast cancer cells. [47]

3.6 Summary

Different size (color) CdSe/ZnS quantum dots were synthesized in organic solvent with high emission quantum yield. Water-soluble luminescent/magnetic particles consisting of a magnetic core (γ-Fe_2O_3) and luminescent quantum dots shell (CdSe/ZnS quantum dots) were synthesized in an organic/water two-phase mixture. Thiol chemistry was used to bind the quantum dots to the surface of the magnetic beads. The luminescent/magnetic nanocomposite particles were characterized using TEM and EDS analysis. The particles averaged 20 nm in diameter with about 15% size variation, showed relatively smooth morphology, and were fully water miscible. They also exhibited high emission quantum yield and were easily separated from solution using a permanent magnet. Anti cycline E molecules against the breast cancer specific marker cycline E, were attached to the luminescent/magnetic particles followed their functionalization with carboxylic groups through EDAC coupling. The anti cycline E labeled particles were used successfully to separate and detect breast cancer cells in serum and in red blood cells.

CHAPTER 4: SUMMARY AND CONCLUSIONS

Luminescent semiconductor quantum dots (QDs) are series of particles whose size ranges from 1.5 to 8 nm. They have very unique properties compared to organic dyes including high quantum yield, sharp fluorescence emission, wavelength tunable emission, broad excitation range and high photostability. CdSe QDs have fluorescence emission that lies in visible light range (450-700 nm) due to its bandgap. They were synthesized in organic solvent trioctylphosphine oxide (TOPO) with surfactant hexadecylamine (HDA). After being coated with ZnS, their quantum yield, stability and emission can be dramatically enhanced with a little red shift. The larger bandgap of ZnS layer decrease the electron leaking from CdSe core which enhances the fluorescence efficiency. The quantum yield can be increased up to 100% with a novel synthesis method ─ one-pot synthesis. [47] The surface of CdSe/ZnS can be modified with different carboxylic ligands such as mercaptoacetic acid, mercaptosuccinic acid, etc which make them water-soluble and biological compatible. The water-soluble CdSe/ZnS QDs still kept high and sharp fluorescence emission with a little blue shift.

CdSe/ZnS QDs were successfully coated onto the surface of magnetic particles (γ-Fe_2O_3) which were coated with DMSA in a organic and inorganic solvents mixture (chloroform:methanol:water=10:5:1). The magnetic particles can be made from ferrofluid

by modifying with DMSA. The mechanism is thiol binding at the expense of Fe releasing from the magnetic particle surface. There are free carboxylic and thiol groups on the surface of magnetic particles (Thiol:Carboxy=30:200). The connection between CdSe/ZnS QDs and magnetic particles is thiol binding to metal. It is a stable coating. Strong, sharp fluorescence emission of CdSe/ZnS QDs was remained. The number of QDs on the coating layer depends on both the size of magnetic particles and QDs, ranging from 45 to 133 for a 10 nm magnetic particle when the QD diameter decreases from 4 to 2 nm. The water-solubility of those luminescent/magnetic particles can be further improved with mecaptoacetic acid.

The biological applications of luminescent/magnetic particles are promising. Preliminary cell separations from suspension and red blood cell mixture were successful. In order to attach luminescent/magnetic particles to MCF-7 breast cancer cells, anti cycline E was attached to on the surface through EDAC coupling in PBS buffer solution (PH=7.4). As a result, the particles were able to bind cells through antibody-antigen recognition and a magnet can pull out the cells from the suspension. Further experiment proved that MCF-7 cells could be separated from a mixture of red blood cells and MCF-7 breast cancer cells. Fluorescence images of cells on microscope showed high resolution. Preliminary measurements indicate that the technique can be used to separate one MCF-7 cell in 10,000 red blood cells. We anticipate that technical improvements in the experimental system would increase the separation efficiency furthermore.

REFERENCES

1. Alivisatos, A. P. *Science* **1996**, 217, 933
2. Murray, C. B.; Norris, D. J.; Bawendi, M. G. *J. Am. Chem. Soc.* **1993**, 115, 8706-8715
3. Donegá, C. M.; Hickey, S. G.; Wuister, S. F.; Vanmaekelbergh, D.; Meijerink, A. *J. Phys. Chem. B* **2003**, 107, 489-496
4. Peng, Z. A and Peng, X. *J. Am. Chem. Soc*. **2001**, 123, 183-184
5. Cohen, R.; Kronik, L.; Shanzer, A.; Cahen, D.; Liu, A.; Rosenwaks, Y.; Lorenz, J. K; and Ellis, A. B. *J. Am. Chem. Soc*. **1999**, 121, 10545-10553
6. Murray, C.; Kagan, C.; Bawendi, M. *Annu. Rev. Mater. Sci*. **2000**, 30, 546-610
7. Brus, L. *Appl. Phys. A; Mater, Sci. Process* **1991**, 53, 465-474
8. Warren C. W. and Nie, S. *Science*, **1998**, 281, 2016–2018
9. Http://www.qdots.com/new/technology/what.html
10. Murphy, C. J. *Anal. Chem.* **2002**, Oct 1, 520A-526A
11. Rajeshwar, K.; Tacconi, N. R.; and Chemthamarakshan, C. R. *Chem. Mater.* **2001**, 13, 2765-2782
12. Trindade, T.; O'Brien, P. and Pickett, N. L. *Chem. Mater*. **2001**, 13, 3843-3858
13. Nazzal, A. Y.; Qu, L.; Peng, X. and Xiao, M. *Nano Letters*, **2003**, 3(6), 819-822

14. abbousi, B. O.; Rodriguez-Viejo, J.; Mikelec, F. V.; Heine, J. R.; Mattoussi, H.; Ober, R.; Jensen, K. F. and Bawendi, M. G. *J. Phys. Chem. B* **1997**, 101, 9463-9475
15. Gerion, D.; Pinard, F.; William, S. C.; Parak, W. J.; Zanchet, D.; Weiss, S. and Alivisatos, A. P. *J. Phys. Chem. B* **2001**, 105, 8861-8871
16. Wuister, S. F.; Swart, I.; Driel, F. V.; Hickey, S. G. and Donegá, C. M. *Nano letters*, **2003**, 3(4), 503-507
17. Chen, Y. and Rosenzweig, Z. *Nano letters*. **2002**, 2(11), 1299-1302
18. Chen, Y.; Ji, T. and Rosenzweig; Z. *Nano Letters*. **2003**, 3 (5), 581-584
19. Wang, Y. A.; Li, J. J.; Chen, H. and Peng, X. *J. Am. Chem. Soc*. **2002**, 124(10), 2002
20. Zhang, C.; O'Brien, S. and Balogh, L. *J. Phys. Chem*. B **2002**, 106, 10316-10321
21. Personal discussion with Professor Alivisatos
22. Danek, D.; Jensen, K. F.; Murray, C. B. and Bawendi, M. G. *Chem. Mater*. **1996**, 8, 173-180
23. Hines, M. A.; Guyot-Sionnest, P. *J. Phys. Chem.* **1996**, *10*0, 468.
24. Hines, M. A. and Guyot-Sionnest, P. *J. Phys. Chem.* **1996**, 100, 468-471
25. Aldana, J.; Wang, Y. A.; Peng, X. *J. Am. Chem. Soc*. **2001**; *123*(36); 8844-8850.
26. Guo, W.; Li, J. J.; Wang, A. and Peng, X. *Chem. Mater.*, **2003,** 15 (16), 3125 - 3133,
27. Danek, M.; Jensen, K. F.; Murray, C. B.; Bawendi, M. G. *J. Cryst. Growth.* **1994**, 145, 714

28. wang, Y.; Herron, N. *J. Phys. Chem*. **1991**, 95, 525

29. Li, X.; Fryer, J. R.; Cole-hamilton, D. J. *Chem. Commun*. **1994,** 1715

30. Wang, Y.; Herron, N.; Mahler, W.; Suna. A. *J. Opt. Soc. Am*. B **1989**, 6 808

31. Hagfeldt, A.; Grätzel, M. *Chem. Rev*. **1995**, 7, 607

32. Henglein, A.; Gutierrez, M.; Fisher, Ch. H. Ber. Bunsen-Ges. *Phys. Chem*. **1984**, 88, 170

33. Jaiswal, J. K.; Mattoussi, H.; Mauro, J. M. and SimonS. M. *Nature. Biotech*. **2003**, 21 47-51

34. Murphy, C. J.; *Anal. Chem*. **2002**, Oct 1, 520A-526A

35. Chan, C. W. and Nie, S. *Science*, **1998**, 25, 2016-2018

36. Kumar, K. N. P.; Keizer, K.; Burggraaf, A. J.; Okubo, T.; Nagamoto, H.; Morooka, S. *Nature* **1992**, 48, *358*

37. Sberveglieri, G.; Depero, L. E.; Ferroni, M.; Guidi, V.; Martinelli, G.; Nelli, P.; Perego, C.; Sangaletti, L. *Adv. Mater*. **1996**, *8*, 334.

38. Goldman, E. R.; Anderson, G. P.; Tran, P. T.; Mattoussi, H.; Charles, P. T.; Mauro, J. M. *Anal. Chem*. **2002**, *74(4);* 841-847.

39. Goldman, E. R.; Balighian, E. D.; Mattoussi, H.; Kuno, M. K.; Mauro, J. M.; Tran, P. T.; Anderson, G. P. *J. Am. Chem. Soc.* **2002**; *124*(22); 6378-6382.

40. Han, M. Y.; Gao, X. H.; Su, J. Z.; Nie, S. *Nature Biotech*. **2001**, 19(7): 631-635

41. Ji, J.; Rosenzweig, N.; Griffin, C.; Rosenzweig, Z.; *Anal. Chem*. **2000**, 72(15), 3497-3503

42. Jochen Weiss and D. Julian McClements. *J. Agric. Food Chem*., **2001** 49 (9), 4372 –4377

43. Srikant Pathak, Soo-Kyung Choi, Norman Arnheim, and Mark E. Thompson. *J. Am. Chem. Soc.* **2001**, 123, 4103-4104

44. Cumberland, S. L.; Berrettini, M. G.; Javier, A. and Strouse, G. F. Chem. Mater. **2003**, 15, 1047-1056

45. Van Sark, W. G. J. H. M.; Frederix, P. L. T. M.; Van den Heuvel, D. J.; Gerritsen, H. C.; Bol, A. A.; van Lingen, J. N. J.; de Mello Donega, C.; Meijerink, A.; *J. Phys. Chem*. B **2001**, 105, 8281-8284

46. Zymed Technote: *http://www.zymed.com*

47. D. Wang, J. He, N. Rosenzweig and Z. Rosensweig. *Nano Letters* **2004** 4(3) 409-413

48. Fisher, B. R.; Hans-Jurgen, E.; Nathan, E. S.; Bawendi, M. G. *J.Phys. Chem. B* **2003**, *108*, 143-148.

49. Tortora, G.; Funke, B.; Case, C. L. *Microbiology*, 5th ed.; The Benjamin/Cummings Publishing Co. Inc.: Reading, MA, **1995**; pp 413-414.

50. Martinez-Cayuela, M. *Biochimie* **1995**, 77, 7-161.

51. Lo, Y. Y.; Cruz, T. F. *J. Biol. Chem*. **1995**, 270 (20), 11727-11730.[ChemPort]

52. McIlroy, B. W.; Curnow, A.; Buonaccorsi, G.; Scott, M. A.; Brown, S. G.; MacRobert, A. *J. Photochem. Photobiol. B: Biol*. **1998**, 43, 47-55.[ChemPort]

53. Glickson, J. J., Wehrle, J. P., Rajan, S. S., Li, S. J., Steen, R. G., Pettegrew, J. W., Eds. NMR spectrocscopy of tumors. In NMR: *Principles and Applications to Biomedical Research;* Springer-Verlag: New York, **1990**; pp 255-309.

54. N. Fauconnier; J. N. Pons; J. Roger and A. Bee. *Journal of Colloid and Interface Science* 194, 427-433 (**1997**)

55. C. Wilhelm; F. Gazeau; J. Roger; J. N. Pons and J. C. Bacri. *Langmuir* **2002**, 18, 8148-8155

56. Kara E. McCloskey; Jeffrey J. Chalmers and Maciej Zborowski. *Anal. Chem*. **2003**, 75, 6868-6874

57. Xiao-Dong Tong, Bo Xue, and Yan Sun. *Biotechnol. Prog*. **2001**, 17, 134-139

58. Kara E. McCloskey; Lee R. Moore; Mauricio Hoyos; Alex Rodriguez; Jeffrey J. Chalmers and Maciej Zborowski, *Biotechnol. Prog*. **2003**, 19, 899-907

59. K. Bu¨ scher; C. A. Helm; C. Gross; G. Glo¨ckl; E. Romanus and W. Weitschies. *Langmuir*, **2003**

60. Nuria O. Nu´n˜ez; Pedro Tartaj; M. Puerto Morales; Raul Pozas; Manuel Ocan˜a and Carlos J. Serna. *Chem. Mater*. **2003**, 15, 3558-3563

61. Pedro Tartaj; Teresita Gonza´lez-Carren˜o and Carlos J. Serna. *Langmuir* **2002,** 18, 4556-4558

62. Yongfen Chen *Doctoral Dissertation*

63. Colvin, V. L.; Schlamp, M. C.; Alivisatos, A. P. *Nature* **1994**, *370*, 354

VITA

The author was born in Shandong, China. He obtained his B.S. in Chemistry Department of Nankai University, China in 1997. In 2001, he joined the Department of Chemistry at the University of New Orleans and became a member of Professor Zeev Rosenzweig's research group.